# Asymptotes and Asymptotic Analysis for Development of Compact Models for Microelectronics Cooling

**M. Michael Yovanovich**
Distiniguished Professor Emeritus
Principal Scientific Advisor
Microelectronics Heat Transfer Laboratory
University of Waterloo, ON, Canada
email: mmyov@mhtlab.uwaterloo.ca.

*Abstract*— **In the thermal analysis of microelectronic systems various levels of compact models are required to bridge the gap between the use of simple correlation equations which give quick, partial solutions and the use of costly, time consuming, numerical methods which give complete solutions with much detail. There are various levels of compact models: some are based on simple combinations of two or more correlation equations; some are based on resistor networks; and some are based on various combinations of asymptotic solutions. This paper shows that many different complex physical problems, when they are nondimensionalized, exhibit similar trends, i.e., that the complex solution varies smoothly between two asymptotic solutions. Rules are presented for the method of combining the asymptotes and how to calculate the "fitting" parameter. One example shows how to develop a compact model for steady conduction across a gas layer for very small and very large Knudsen numbers. A compact model for predicting the complex elastic-plastic contact between a hard sphere and a softer substrate is presented. This elastic-plastic contact model is required for development of the thermal spreading-constriction model. Another example shows how to model the effect of very small and very large Prandtl numbers for forced and natural convection from isothermal plates. Examples are given from forced and natural convection in short and long ducts and pipes of arbitrary cross section for uniform wall temperature and wall heat flux. The simple compact models are found to be accurate when compared with numerical results and experimental data, and they are easy to implement.**

*Keywords*— **Asymptotes, asymptotic analysis, compact models, steady and transient conduction, radiation, rarefaction, contact mechanics, elastic, plastic, elastic-plastic, forced and natural convection.**

**Nomenclature**

| | | |
|---|---|---|
| $A$ | = | flow area, $m^2$ |
| $a$ | = | contact radius, $m$ |
| $a, b$ | = | semi major and minor axes of ellipse, $m$ |
| $a, b$ | = | half dimension of rectangle, $m$ |
| AR | = | aspect ratio |
| $c_i$ | = | constants, $i = 1...5$ |
| $c_P$ | = | specific heat, $J/kgK$ |
| $D$ | = | gap thickness, $m$ |
| $D_h$ | = | hydraulic diameter $4A/p$, $m$ |
| $E_1, E_2$ | = | Young's modulus, $Pa$ |
| $f$ | = | friction factor, $2\tau/\rho v^2$ |
| $F$ | = | load, $N$ |
| $F_0$ | = | dimensionless time, $\alpha t/A^2$ |
| $F\,(\mathrm{Pr})$ | = | Prandtl number function |
| $g$ | = | gravitational constant, $m/s^2$ |
| $G$ | = | body gravity function |
| $G$ | = | dimensionless reciprocal flux, $1/q^*$ |
| $h$ | = | heat transfer coefficient, $W/m^2K$ |
| $H_B$ | = | Brinell hardness, $N/m^2$ |
| $k$ | = | thermal conductivity, $W/mK$ |
| $Kn$ | = | Knudsen number, $\Lambda/D$ |
| $L$ | = | length of tube, pipe, duct, $m$ |
| $L_\lambda$ | = | optical path length, $m$ |
| $\mathcal{L}$ | = | arbitrary length scale, $m$ |
| $m, n$ | = | exponents of dimensionless solutions |
| $M$ | = | gas parameter, $\alpha\beta\Lambda$ |
| $Nu$ | = | Nusselt number, $hL/k$ |
| $p$ | = | fitting parameter |
| $P$ | = | perimeter, $m$ |
| $P$ | = | gas pressure, $Pa$ |
| $Pr$ | = | Prandtl number, $\nu/\alpha$ |
| $Q$ | = | heat transfer rate, $W$ |
| $Q_L^*$ | = | dimensionless heat flow, $Q\mathcal{L}/kA\theta_0$ |
| $q$ | = | heat flux, $W/m^2$ |
| $q^*$ | = | dimensionless heat flux |
| $r$ | = | radius, $m$ |
| Re | = | Reynolds number, $U\mathcal{L}/\upsilon$ |
| Ra | = | Rayleigh number, $g\beta\Delta T\mathcal{L}^3/\alpha\nu$ |
| $S_L^*$ | = | dimensionless shape factor, $Q\mathcal{L}/kA\theta_0$ |
| $t$ | = | time, $s$ |
| $T$ | = | temperature, $K$ |
| $U$ | = | mean velocity, $m/s$ |
| $w$ | = | axial velocity, $m/s$ |

***Greek***

| | | |
|---|---|---|
| $\alpha$ | = | thermal diffusivity, $m^2/s$ |
| $\alpha$ | = | accommodation coefficient |
| $\beta$ | = | gas parameter |
| $\gamma$ | = | ratio of specific heats, $c_p/c_v$ |
| $\gamma$ | = | symmetry parameters |
| $\Delta$ | = | thermal boundary layer thickness, $m$ |
| $\delta$ | = | momentum boundary layer thickness, $m$ |
| $\epsilon$ | = | aspect ratio, $b/a < 1$ |
| $\Lambda$ | = | gas mean free path, $m$ |
| $\mu$ | = | dynamic viscosity, $Ns/m^2$ |

| | | |
|---|---|---|
| $\mu^*$ | = | dimensionless gas parameter, $M/D$ |
| $\nu$ | = | kinematic viscosity, $m^2/s$ |
| $\nu_1, \nu_2$ | = | Poisson's ratio |
| $\rho$ | = | fluid density, $kg/m^3$ |
| $\rho$ | = | radius of curvature, $m$ |
| $\tau$ | = | wall shear stress, $Pa$ |
| $\theta$ | = | temperature excess, $T - T_i$, $K$ |
| $\phi$ | = | dimensionless dependent parameter |
| $\xi$ | = | dimensionless independent parameter |
| $\sigma$ | = | Stephan-Boltzman constant, $5.67E-8$, $W/m^2K^4$ |

***Subscripts***

| | | |
|---|---|---|
| 0 | = | reference values |
| 0 | = | corresponding to very small value |
| $\infty$ | = | corresponding to very large value |
| $1, 2$ | = | surfaces 1 and 2 |
| $\sqrt{A}$ | = | based on square root of area |
| $bl$ | = | boundary layer |
| $c$ | = | critical |
| $D_h$ | = | based on hydraulic diameter |
| $e$ | = | entrance |
| $fd$ | = | fully developed |
| $\mathcal{L}$ | = | based on arbitrary length |
| $R$ | = | radiation |
| $t$ | = | thermal |
| $x$ | = | local value |
| w | = | wall |
| $\lambda$ | = | optical |

## I. Introduction

THE present demands on the thermal analysts who must daily deal with microelectronics cooling issues is daunting. They are required to provide, in very short time, reliable estimates of temperatures within devices, packages, boards and systems which are often cooled by air by either natural or forced flow. Although experiments and numerical methods can be employed to find the temperatures and provide much detail about the temperature distribution throughout the system; these methods are both time consuming and costly. Certainly in the early stages of design, experiments are not feasible and numerical methods may require information that is not readily available. Figure 1 illustrates that the single correlation equations fall in the lower left corner, the numerical results lie in the upper right corner where much detailed information is available at some high cost, and the compact models form the relative large "bridge" between the very low cost and high cost regions. There are many different types of compact models ranging from relatively simple models to relatively complex models.

It is apparent that alternative simpler methods are required in the first stages of device, package and board development to give quick and acceptable estimates of temperature levels. One very simple method is based on the use of correlation equations which have been developed from experimental or numerical data. Often the correlations are limited to the particular ranges of the independent parameters such as Reynolds number or modified Reynolds for forced convection and Rayleigh and modified Rayleigh number for pipe and channel flows, and the Prandtl number if fluids other than air are used.

There is a need for the development simple "compact models" which incorporate one or more asymptotic solutions and which are not limited to particular ranges of the independent parameters. These compact models can therefore be used over broader ranges of the parameters and are more useful and valuable than the simple correlation equations alone.

This paper will be restricted to several relatively simple, but important, compact models which have been applied to some microelectronics cooling problems.

## II. Asymptotes and Simple Compact Model development

Many complex physical systems exhibit a smooth transition between two asymptotic solutions [1,2,3]. The smooth transition means that there are no discontinuities and no sudden changes in slope within the transition region.

These asymptotes appear in steady and transient internal and external conduction, steady conduction across a gas layer between two large parallel isothermal plates, radiation through a highly porous substance between two large isothermal walls, contact between a "rigid" sphere and a softer substrate, natural and forced internal and external convection. There are many other examples from conduction, fluid flow, and mass transfer; however, they will not be considered in this paper.

Since the various problems have different dependent and independent parameters and different symbols are used, it is necessary to present the asymptotes and the method of combining them in a general form based on dimensionless dependent and independent parameters.

The dimensionless dependent parameter is called $\phi$ and the independent parameter is called $\xi$. The functional dependence $\phi(\xi)$ can be relatively simple or quite complex depending on the physical problem.

The dimensionless parameter $\phi$ has two asymptotes corresponding to very small and very large values of the dimensionless independent parameter $\xi$ [1,2,3]:

$$\phi \rightarrow \begin{cases} \phi_0 = C_0\,\xi^m & \text{as} \quad \xi \rightarrow 0 \\ \phi_\infty = C_\infty\,\xi^n & \text{as} \quad \xi \rightarrow \infty \quad \text{or} \quad \xi \rightarrow 1 \end{cases} \tag{1}$$

The asymptotes $\phi_0$ and $\phi_\infty$ are based on analytical solutions and they consist of a constant which is a positive, real number. The two constants are denoted as $C_0$ as $\xi \rightarrow 0$ and as $C_\infty$ for $\xi \rightarrow \infty$ or $\xi \rightarrow 1$. The exponents $m$ and $n$ can have the values such as $0, 1, 1/2, 1/4, 1/3$ for example [1,2,3].

It is known from analysis, experiments and numerical work that $\phi$ frequently transitions in a smooth manner between the two asymptotes.

The plots in Figs. 2 through 5 illustrate four basic, but different, trends. Figure 2 shows both asymptotes $\phi_0$ and $\phi_\infty$ increasing with increasing values of $\xi$, and the solution

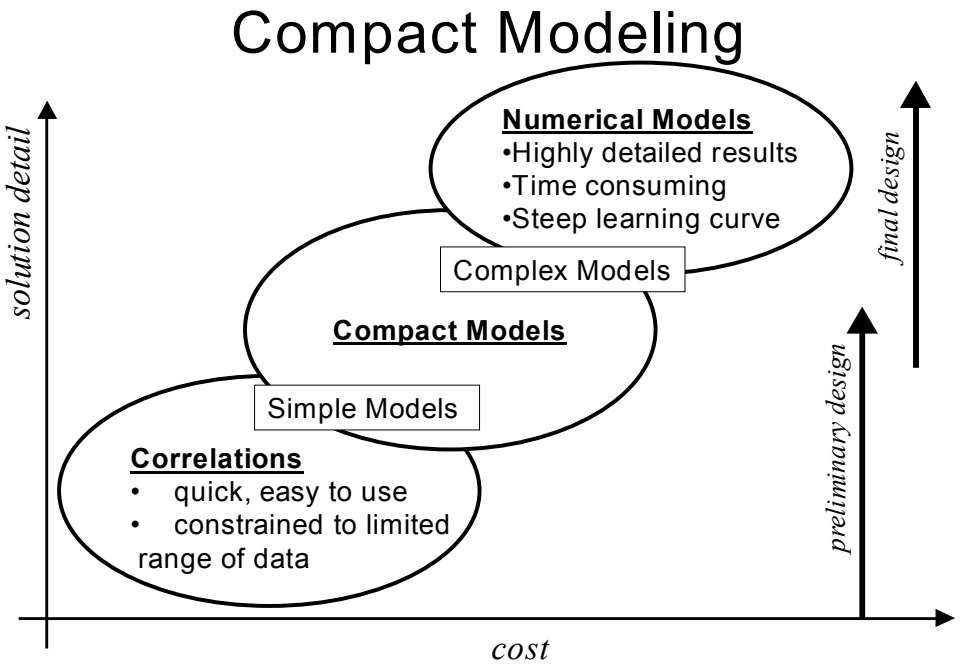


Fig. 1. Overview of Simple, Compact and Detailed Models

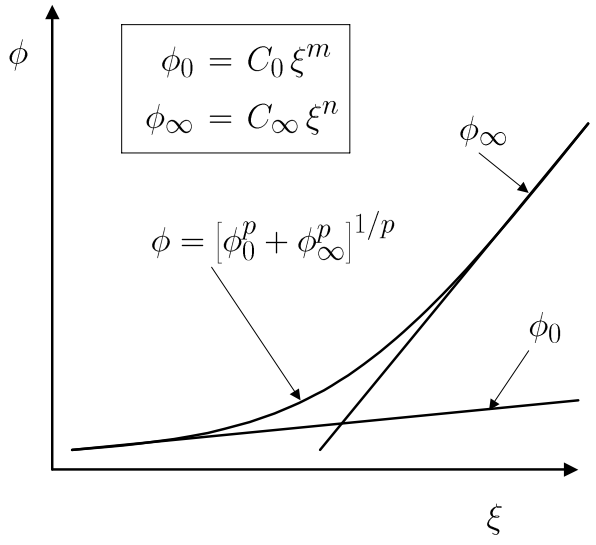


Fig. 2. Asymptotes and Compact Model 1

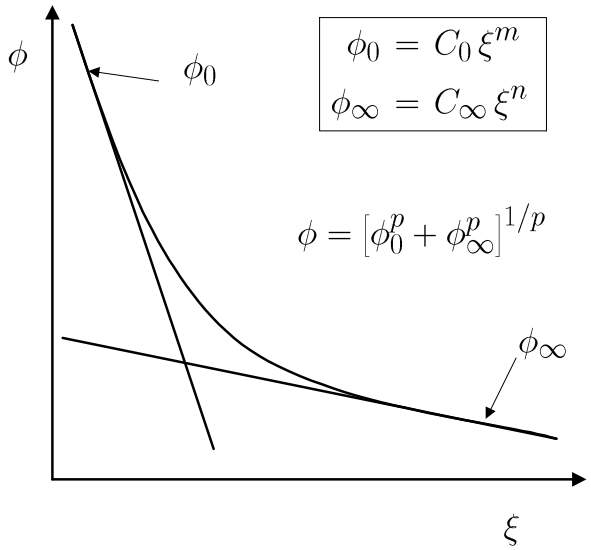


Fig. 3. Asymptotes and Compact Model 2

$\phi$ is *concave upwards*. For example, external forced and natural convection from single isothermal convex bodies exhibit this trend.

Figure 3 shows both asymptotes $\phi_0$ and $\phi_\infty$ decreasing with increasing values of $\xi$, and the solution $\phi$ is *concave upwards*. For example, steady conduction in spherical wall and external transient conduction from isothermal convex bodies exhibit this trend.

Figure 4 shows both asymptotes $\phi_0$ and $\phi_\infty$ increasing with increasing values of $\xi$, and the solution $\phi$ is *concave downwards*. For example, internal forced and natural convection within ducts and channels exhibit this trend.

Figure 5 shows the asymptote $\phi_0$ to be constant independent of $\xi$ and the asymptote $\phi_\infty$ decreases with increasing values of $\xi$, and the solution $\phi$ is *concave downwards*. An example from tribology is the temperature rise of a heated contact area which moves with constant velocity in the surface of a semi-infinite body [4].

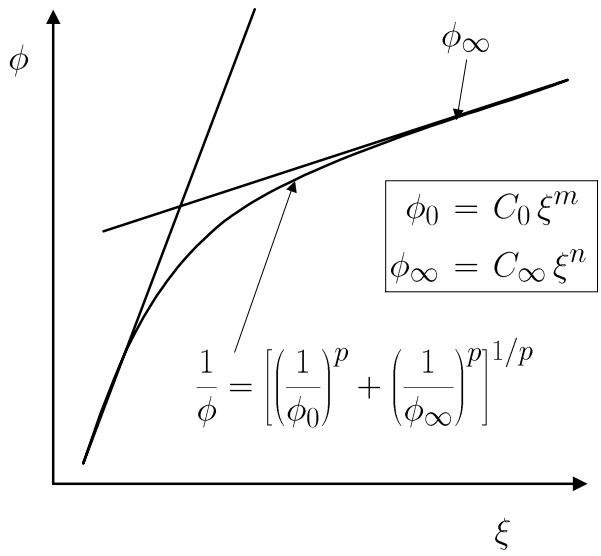


Fig. 4. Asymptotes and Compact Model 3

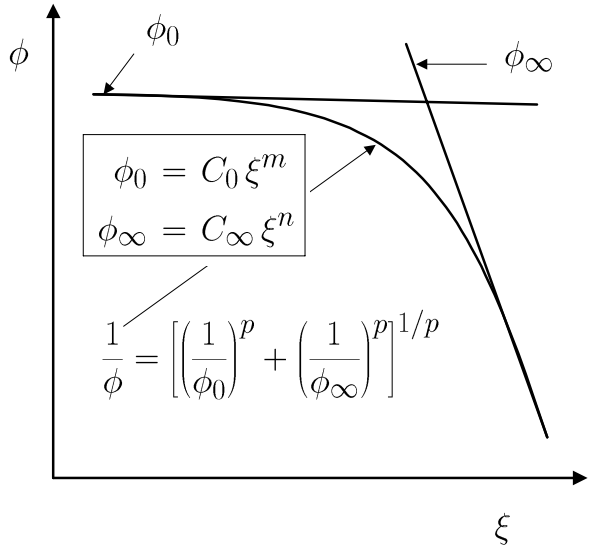


Fig. 5. Asymptotes and Compact Model 4

### *A. Combined or Simple Compact Models*

The asymptotes $\phi_0$ and $\phi_\infty$ can be combined in two different ways depending on the trends of $\phi_0$ and $\phi_\infty$ with respect to $\xi$ [1,2,3].

If $\phi_0 > \phi_\infty$ as $\xi \to 0$, the solution $\phi$ is *concave upwards*, and the asymptotes are combined in the following manner [1,2,3]:

$$\phi = [\phi_0^p + \phi_\infty^p]^{1/p} \tag{2}$$

If $\phi_0 < \phi_\infty$ as $\xi \to 0$, the solution $\phi$ is *concave downwards*, and the asymptotes are combined in the following manner [1,2,3]:

$$\frac{1}{\phi} = \left[\left(\frac{1}{\phi_0}\right)^p + \left(\frac{1}{\phi_\infty}\right)^p\right]^{1/p} \tag{3}$$

The parameter $p$ is a *fitting* parameter whose value can be found in a simple manner.

To find a value of $p$ we can select an intermediate value of $\xi = \xi_i$ for which $\phi(\xi_i)$ is known through analytical, experimental or numerical methods. For the intermediate value of $\xi$ we can write

$$\phi(\xi_i) = [(C_0\xi_i^m)^p + (C_\infty\xi_i^n)^p]^{1/p} \tag{4}$$

or

$$\frac{1}{\phi(\xi_i)} = \left[\left(\frac{1}{C_0\xi_i^m}\right)^p + \left(\frac{1}{C_\infty\xi_i^n}\right)^p\right]^{1/p} \tag{5}$$

In both relationships the "fitting" parameter $p$ is unknown. It can, however, be calculated by numerical methods or by means of computer algebra systems such as Maple, Mathematica, and Mathcad.

### *B. Alternative Forms of Simple Compact Models*

Often the approximate solution is presented in a form which is based on one of the two asymptotes. If this is done, then the two models can expressed as [1,2,3]:

$$\text{model 1} \qquad \phi = \begin{cases} \phi_0\,[1 + (\phi_\infty/\phi_0)^p]^{1/p} \\ \phi_\infty\,[1 + (\phi_0/\phi_\infty)^p]^{1/p} \end{cases} \tag{6}$$

$$\text{model 2} \qquad \phi = \begin{cases} \phi_0/\,[1 + (\phi_0/\phi_\infty)^p]^{1/p} \\ \phi_\infty/\,[1 + (\phi_\infty/\phi_0)^p]^{1/p} \end{cases} \tag{7}$$

Several examples from steady and transient conduction, contact mechanics, forced and natural convection heat transfer will be presented in the following sections to illustrate several features of the asymptotes, asymptotic analysis and the development of simple compact models.

## III. Steady Conduction Across Stationary Gas Layer

The first example illustrates the importance of asymptotes for steady conduction across a stationary gas layer placed between two *infinitely* large parallel isothermal plates. The absolute temperatures of the bounding surfaces are $T_1$ and $T_2$ where $T_2 < T_1$. The layer thickness is $D$, and the thermal conductivity of the gas is $k_g$. The gas pressure is $P$ and the gas temperature is $T = (T_1 + T_2)/2$.

The steady heat flux $q = Q/A$ at the left or right boundaries depends on the thermal conductivity of the gas $k_g$, the temperature drop across the layer $T_1 - T_2$ , the layer thickness $D$, and another thermophysical parameter denoted as $M$ which accounts for *imperfect* heat exchange between the gas molecules and the molecules of the bounding surfaces. The gas-layer parameter is defined as [5,6]

$$M = \alpha\beta\Lambda \tag{8}$$

where $\alpha$, the accommodation parameter, is defined as [7,8]

$$\alpha = \frac{2 - \alpha_1}{\alpha_1} + \frac{2 - \alpha_2}{\alpha_2} \tag{9}$$

and $\alpha_1$ and $\alpha_2$ are the accommodation coefficients for each gas-solid interface. These are complex, dimensionless parameters. The second gas parameter is [5,6]

$$\beta = \frac{2\gamma}{(\gamma+1)\,Pr} \tag{10}$$

where $\gamma = c_p/c_v$, and $Pr = \nu/\alpha$ is the Prandtl number of the gas. The third gas parameter is called the molecular mean free path and its defined as [5,6]

$$\Lambda = \Lambda_0 \left(\frac{T}{T_0}\right)\left(\frac{P_0}{P}\right) \tag{11}$$

The molecular mean free path $\Lambda_0$ is the value at the reference temperature $T_0$ and reference gas pressure $P_0$. Its seen from the relationship that increasing the gas temperature or decreasing the gas pressure increases the molecular mean free path.

Some typical values of gas properties are listed in Table 1. Gas parameter values are for $T_0 = 288\,\mathrm{K}$ and $P_0 = 760\,\mathrm{torr}$ (1 atm).

TABLE I
Typical Values of Gas Parameters

| | $\alpha$ | $\gamma$ | Pr | $k_g$ | $\Lambda_0$ |
|---|---|---|---|---|---|
| Gas | [–] | [–] | [–] | $W/(m\cdot K)$ | $nm$ |
| Argon | 0.90 | 1.67 | 0.67 | 0.0177 | 66.6 |
| Nitrogen | 0.78 | 1.41 | 0.69 | 0.0259 | 62.8 |
| Helium | 0.55 | 1.67 | 0.67 | 0.150 | 186 |

The heat flux is given by the following relationship [5,6,9,10]

$$q = k_g \frac{T_1 - T_2}{D + M} \tag{12}$$

This relationship has two asymptotes depending on the relative magnitude of $M/D$ or $M/D$. The asymptotes are

$$q = \begin{cases} q_0 = k_g \dfrac{T_1 - T_2}{D} & \text{as} \quad \dfrac{M}{D} \to 0 \quad \text{continuum} \\ q_\infty = k_g \dfrac{T_1 - T_2}{M} & \text{as} \quad \dfrac{M}{D} \to \infty \quad \text{free molecules} \end{cases} \tag{13}$$

The two heat flux asymptotes $q_0$ and $q_\infty$ depend on the dimensionless parameter $M/D$ which can be expressed as [5,6]

$$M^\star = \frac{M}{D} = \alpha\beta\frac{\Lambda}{D} = \alpha\beta Kn \tag{14}$$

where $Kn = \Lambda/D$ is called the Knudsen number for the gas layer. The Knudsen number depends on the temperature and the pressure of the confined gas.

We can nondimensionalized the heat flux such that

$$q^\star = \frac{qD}{k_g\,(T_1 - T_2)} \tag{15}$$

The dimensionless heat flux has the following two dimensionless asymptotes:

$$q^\star = \begin{cases} q_0^\star = 1 & \text{as} \quad Kn \to 0 \\ q_\infty^\star = \dfrac{D}{M} = \dfrac{1}{M^\star} & \text{as} \quad Kn \to \infty \end{cases} \tag{16}$$

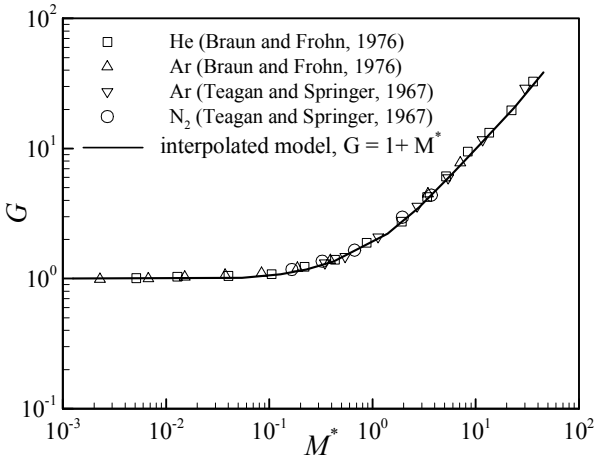


Fig. 6. Comparison of Data and Compact Model for Conduction Across Gas Layer

We now set $\phi = q^\star$, $\xi = M^\star$, $\phi_0 = 1$ and $\phi_\infty = 1/\xi$. Plots of the two asymptotes show that $\phi_0 > \phi_\infty$ as $\xi \to 0$, and the solution is cave downwards. This trend corresponds to the example shown in Fig. 5 and, therefore, the simple compact model is given by Eq. (3). The dimensionless parameters, the constants and the exponents for the asymptotes are listed in Table 2.

TABLE II
Parameters for Conduction Across Stationary Gas Layer

| $\phi$ | $\xi$ | $C_0$ | $m$ | $C_\infty$ | $n$ | $p$ |
|---|---|---|---|---|---|---|
| $\dfrac{qD}{k_g\,(T_1 - T_2)}$ | $\dfrac{M}{D}$ | 1 | 0 | 1 | 1 | $-1$ |

The alternative relationship for the heat flux is

$$\frac{1}{q} = \frac{D+M}{k_g\,(T_1 - T_2)} = \frac{D}{k_g\,(T_1 - T_2)} + \frac{M}{k_g\,(T_1 - T_2)} \tag{17}$$

This relationship clearly shows how the two asymptotes for the heat flux combine to give the compact model for conduction across the gas layer. The non-dimensional form is

$$\frac{1}{q^\star} = \frac{1}{q_0^\star} + \frac{1}{q_\infty^\star} = 1 + \frac{M}{D} = 1 + \frac{1}{M^\star} \tag{18}$$

This form is consistent with that given by the general model for combining asymptotes. This relationship shows that the "fitting" parameter must be $p = 1$ in Eq. (3).

The simple compact model was compared against data obtained for Argon, Nitrogen and Helium or a wide range of the parameter $M/D$. Song [5] and Song et al. [6] defined $G = 1/q^\star$ which was called the dimensionless gap resistance and $M^\star = M/D$ which was called the gas rarefaction parameter, and compared the simple gas-layer model expressed as

$$G = 1 + M^\star \tag{19}$$

against the experimental data obtained for Argon, Nitrogen and Helium as shown in Fig. 6 for a wide range of the

dimensionless gas-layer parameter $M^\star$. The Argon and Nitrogen data [9] and the Argon and Helium data [10] are seen to lie in the continuum regime for $M^\star < 0.1$, the free molecule regime for $M^\star > 10$ and in the transition. The agreement between the simple gas layer conduction model and all data is excellent.

## IV. Simple Model for Radiation Through Porous Substance

In this example we examine steady heat transfer by radiation through a porous layer of thickness $L$. The problem and its solution is given in Gebhart [11].

The optical path length $L_\lambda$ may be very small, i.e., $L_\lambda/L << 1$, or very large, i.e., $L_\lambda/L >> 1$ relative to the layer thickness. If $L_\lambda/L << 1$, the material is said to be opaque, and if $L_\lambda/L >> 1$, the material is said to be nonopaque. If the material is assumed to be gray, $L_\lambda$ is not a function of $\lambda$ and we set $L_\lambda = \ell$. There are two models corresponding to the magnitude of the parameter $\ell/L$. The layer is assumed to be in contact with two isothermal black "infinitely" large surfaces whose absolute temperatures are $T_1$ and $T_2$ with $T_1 > T_2$.

### *A. Thin Layer Asymptote: Nonopaque Material*

For very thin layers the net radiation transport across the layers is given by [11]

$$q_\infty = \sigma\left(T_1^4 - T_2^4\right) \qquad \text{for} \quad \frac{\ell}{L} >> 1 \tag{20}$$

where $\sigma$ is the Stefan-Boltzmann constant.

### *B. Thick Layer Asymptote: Opaque Material*

For very thick layers, the radiation transport in the gray material is by local radiation and absorption. The layer is locally nearly in radiant equilibrium. The transport process is analogous to conduction, and the local net radiation flux is [11]:

$$q_0 = -k_R \frac{dT}{dx} \tag{21}$$

where

$$k_R = CT^3 \qquad \text{and} \quad C = \frac{16}{3}\ell\sigma T^3 \tag{22}$$

The differential equation and its solution are presented in [11]. The heat flux for this limit is [11]

$$q_0 = \frac{4}{3}\frac{\ell}{L}\sigma\left(T_1^4 - T_2^4\right) \tag{23}$$

showing the $\ell/L$ dependence. To illustrate the transport rates, we introduce the dimensionless radiation flux

$$q^\star = \frac{q}{\sigma\left(T_1^4 - T_2^4\right)} \tag{24}$$

The dimensionless radiation flux asymptotes are

$$q^\star = \begin{cases} q_0^\star = \dfrac{4}{3}\dfrac{\ell}{L} & \text{as} \quad \dfrac{\ell}{L} \to 0 \\ q_\infty^\star = 1 & \text{as} \quad \dfrac{\ell}{L} \to \infty \end{cases} \tag{25}$$

Comparison of this problem with the general model shows that $\phi = q^\star$, $\phi_0 = q_0^\star$, $\phi_\infty = q_\infty^\star$, and $\xi = \ell/L$. These parameters and the corresponding constants and the exponents are listed in Table 3. Plots of the asymptotes with

TABLE III
Parameters for Radiation Through Porous Layer of Material

| $\phi$ | $\xi$ | $C_0$ | $m$ | $C_\infty$ | $n$ | $p$ |
|---|---|---|---|---|---|---|
| $\dfrac{q}{\sigma\left(T_1^4 - T_2^4\right)}$ | $\dfrac{\ell}{L}$ | 4/3 | 1 | 1 | 0 | 1 |

respect to $\xi$ show that $\phi_0 < \phi_\infty$ as $\xi \to 0$, and the solution is concave downwards. The approximate solution is therefore the second model, Eq. (3).

The approximate model for $q^\star$ is, therefore,

$$\frac{1}{q^\star} = \left[\left(\frac{1}{q_0^\star}\right)^p + \left(\frac{1}{q_\infty^\star}\right)^p\right]^{1/p} \tag{26}$$

A number of analyses have indicated the behavior of $q^\star$ in the intermediate range which lies between the asymptotes. An approximate result by Probstein [11] which is in agreement with the exact analysis is

$$q^\star = \frac{1}{1 + \dfrac{3}{4}\dfrac{\ell}{L}} \tag{27}$$

This indicates that the "fitting" parameter is $p = 1$.

## V. Steady Conduction in a Spherical Enclosure

Steady conduction occurs in a spherical wall having radii $a, b$ with $a < b$, and constant thermal conductivity $k$. The inner and outer boundaries are maintained at uniform and constant temperatures $T_1$ and $T_2$, respectively, with $T_1 > T_2$. The temperature in the spherical wall is steady and radial, $T(r)$.

The governing differential equation in spherical coordinates is

$$\frac{1}{r^2}\frac{d}{dr}\left(r^2\frac{dT}{dr}\right) = 0 \qquad a < r < b \tag{28}$$

The boundary conditions are

$$r = a, \quad T = T_1 \qquad \text{and} \qquad r = b, \quad T = T_2 \tag{29}$$

The solution, in a convenient nondimensional form, is

$$\frac{T - T_2}{T_1 - T_2} = \frac{1/r - 1/b}{1/a - 1/b} \qquad a \le r \le b \tag{30}$$

Alternative forms of the solution are given in texts on conduction [12] and heat transfer [13,14].

The heat transfer rate into the spherical wall at the inner boundary is found from

$$Q = 4\pi a^2\left[-k\frac{dT}{dr}\right]_{r=a} \tag{31}$$

The conduction [12] and heat transfer texts [13,14] present the result in the following forms:

$$Q = \frac{4\pi k\,(T_1 - T_2)\,ab}{b-a} \qquad \text{or} \qquad Q = \frac{4\pi k\,(T_1 - T_2)}{1/a - 1/b} \quad (32)$$

which do not show the very thin and very thick wall asymptotes explicitly.

If the spherical wall is *infinitely* thick, i.e., $b/a \to \infty$, then the relationship for the spherical wall goes to the relationship for the isolated sphere:

$$Q = 4\pi ak\,(T_1 - T_2) \quad (33)$$

The traditional relationships for $Q$ do not reveal other very important features of the solution that can be used to model other systems such as steady conduction in an enclosure formed by two concentric isothermal cubes, for example.

If we introduce the wall thickness $L = b - a$ into the relationship for $Q$, and after some algebraic manipulations we obtain the new, more interesting, relationship:

$$Q = 4\pi a^2 k\left(\frac{T_1 - T_2}{L}\right) + 4\pi a^2 k\left(\frac{T_1 - T_2}{a}\right) \quad (34)$$

The new relationship shows that the heat transfer rate into the spherical wall consists of two terms which become very important depending on the relative magnitude of the wall thickness $L$ to the inner radius $a$. The new relationship clearly shows that the heat transfer rate into the spherical wall has two asymptotes which are:

$$Q = \begin{cases} Q_0 = 4\pi a^2 k\left(\dfrac{T_1 - T_2}{L}\right) & \text{as} \quad \dfrac{L}{a} \to 0 \\ Q_\infty = 4\pi a^2 k\left(\dfrac{T_1 - T_2}{a}\right) & \text{as} \quad \dfrac{L}{a} \to \infty \end{cases} \quad (35)$$

The relationship for $Q$ can be made nondimensional with respect to some system length scale denoted as $\mathcal{L}$ to give:

$$Q^\star = \frac{Q\mathcal{L}}{A_i k\,(T_1 - T_2)} \quad (36)$$

where $A_i = 4\pi a^2$ is the surface area of the inner sphere. The nondimensional form of the relationship is, therefore,

$$Q^\star = \frac{\mathcal{L}}{L} + \frac{\mathcal{L}}{a} \quad (37)$$

There are three system length scales; the two radii and the wall thickness. We cannot select $b$ or $L$ because they both become infinitely large in one limit. Therefore, we must select a length scale associated with the inner sphere. We can select its radius or the square root of the inner surface area which is more convenient for subsequent modeling. If we select $\sqrt{A_i} = 2\sqrt{\pi}a$ set to $\mathcal{L}$ [15,16], then we get the analytical relationship:

$$Q^\star = \frac{\sqrt{A_i}}{L} + 2\sqrt{\pi} \qquad \text{for} \quad 0 < \frac{L}{\sqrt{A_i}} < \infty \quad (38)$$

A plot of $Q^\star$ versus $L/\sqrt{A_i}$ shows that this relationship has two asymptotes corresponding to the very thin and the very thick walls; they are

$$Q^\star = \begin{cases} Q_0^\star = \dfrac{\sqrt{A_i}}{L} & \text{as} \quad \dfrac{L}{\sqrt{A_i}} \to 0 \\ Q_\infty^\star = 2\sqrt{\pi} & \text{as} \quad \dfrac{L}{\sqrt{A_i}} \to \infty \end{cases} \quad (39)$$

For this example the two asymptotes are linearly combined to give the complete model for the spherical wall.

Comparison with the general model shows that $\phi = Q^\star$, $\phi_0 = Q_0^\star$, $\phi_\infty = Q_\infty^\star$ and $\xi = \sqrt{A_i}/L$. Plots of the two asymptotes with respect to $\xi$ show that $\phi_o > \phi_\infty$ as $\xi \to 0$. Since the solution is concave upwards, the first model, Eq. (2), must be use with $p = 1$, which is in agreement with the analytical relationship.

The dimensionless parameters and the corresponding constants and exponents are listed in Table 4.

TABLE IV
Parameters for Steady Conduction in Spherical Wall

| $\phi$ | $\xi$ | $C_0$ | $m$ | $C_\infty$ | $n$ | $p$ |
|---|---|---|---|---|---|---|
| $Q^\star$ | $\sqrt{A_i}/L$ | 1 | 1 | $2\sqrt{\pi}$ | 0 | 1 |

## VI. Model for Enclosures Formed by Two Isothermal Concentric Boundaries

The analytical result found for the enclosure formed by two concentric isothermal spheres can be used to develop approximate models for other enclosures such as one formed by concentric cubes for which there is no analytical solution. The three-dimensional temperature field in the enclosure formed by two concentric cubes is complex, and the heat flux distribution over all surfaces of the inner isothermal cube is also highly nonuniform. The maximum heat flux values occur along the edges and the corners of the cube.

The simple compact model for the cube-in-cube enclosure can be expressed as

$$Q^\star = \left[\left(\frac{\sqrt{A_i}}{L}\right)^p + (Q_\infty^\star)^p\right]^{1/p} \quad (40)$$

The nondimensional heat transfer rate from an isolated cube was found by numerical methods to be $Q_\infty^\star = 3.391$ which is close to the analytical value for the isothermal sphere which is $Q_\infty^\star = 2\sqrt{\pi} = 3.545$ [15,16] which is approximately 4.5% larger. If the inner cube has side dimensions $L_i$ and the outer cube has side dimensions $L_o$, then the geometric parameters for the approximate model are

$$\sqrt{A_i} = \sqrt{6}L_i \qquad L = \frac{L_o - L_i}{2} \qquad \frac{\sqrt{A_i}}{L} = \frac{2\sqrt{6}}{L_o/L_i - 1} \quad (41)$$

The simple compact model for the cube-in-cube enclosure can be expressed in terms of the side dimension ratio as

$$Q^\star = \left[ \left( \frac{2\sqrt{6}}{L_o/L_i - 1} \right)^p + (3.391)^p \right]^{1/p} \tag{42}$$

By trial and error the *fitting* parameter value was found to be $p = 1.070$. The comparisons between the numerical values and those obtained from the approximate models with $p = 1$ and $p = 1.070$ are listed in Table 5.

TABLE V
Comparisons of Numerical Values and Values from Two Approximate Models

| $L_o/L_i$ | numerical | model 1 | model 2 |
|---|---|---|---|
| 1.2 | 27.52 | 27.89 | 27.24 |
| 1.5 | 12.77 | 13.19 | 12.71 |
| 2.0 | 7.87 | 8.29 | 7.93 |
| 5.0 | 4.45 | 4.62 | 4.45 |
| 10 | 3.89 | 3.94 | 3.84 |
| 50 | 3.52 | 3.49 | 3.46 |

All values from the first compact model, with the exception of the last point, lie above the numerical values. The maximum and average differences between the numerical values and the first approximate model with $p = 1$ are 5.4% and 2.3%, respectively. The maximum and average differences between the numerical values and the second compact model with $p = 1.070$ are reduced to about 1.7% and 0.03%, respectively.

The simple compact model developed for the cube-in-cube enclosure can be used for any enclosure in which the gap thickness is uniform. For example, it has been used for enclosures formed by two concentric finite circular cylinders, and other geometries. The asymptote for very thin gaps is unchanged; however, the value for the very thick asymptote must be modified slightly to account for the shape and aspect ratio of the inner body. The agreement between the numerical values and the simple compact model values where found to be close.

If the gap thickness varies with position, a more complex model is required to account for the regions of the enclosure where the gap thickness is very small.

## VII. Transient Conduction External to Isothermal Spheres

A sphere of radius $a$ is placed in a large stationary medium whose thermophysical properties, $k$, the thermal conductivity, and $\alpha$, the thermal diffusivity are constant.

Initially, the temperature of the sphere and the surroundings is $T_i$ everywhere. Suddenly the surface temperature of the sphere is raised to uniform and constant temperature $T_0$ such that $T_0 > T_i$ for all $t > 0$.

The temperature field external to the sphere $r > a$ is transient and radial, $T(r, t)$. The temperature excess $\theta = T(r, t) - T_i$ is the solution of the one-dimensional diffusion equation which, in spherical coordinates, is [12]

$$\frac{1}{r^2}\frac{\partial \theta}{\partial r}\left( r^2 \frac{\partial \theta}{\partial r} \right) = \frac{1}{\alpha}\frac{\partial \theta}{\partial t}, \qquad r > a, \quad t > 0 \tag{43}$$

The initial condition is

$$t = 0, \qquad r \geq a, \qquad \theta(r, 0) = 0 \tag{44}$$

The boundary conditions are

$$\text{for} \quad t > 0, \qquad \theta(r, t) = \theta_0 \quad \text{at} \quad r = a \tag{45}$$

$$\text{for} \quad t > 0, \qquad \theta(r, t) \to 0 \quad \text{as} \quad r \to \infty \tag{46}$$

The solution is given in [12]:

$$\theta = \frac{\theta_0 a}{r} \operatorname{erfc}\left( \frac{r - a}{2\sqrt{\alpha t}} \right) \qquad t > 0, \quad r \geq a \tag{47}$$

where $\operatorname{erfc}(\cdot)$ is the complementary error function. The temperature gradient on the surface of the sphere is [12]

$$\left[ -\frac{\partial \theta}{\partial r} \right]_{r=a} = \frac{\theta_0}{a} + \frac{\theta_0}{\sqrt{\pi}\sqrt{\alpha t}}, \qquad t > 0 \tag{48}$$

The temperature gradient consists of two terms: a term which is constant with respect to time and its related to the sphere radius $a$, and a second term which is related to the thermal penetration thickness $\sqrt{\alpha t}$. The temperature gradient, therefore, consists of two asymptotes: the small penetration depth asymptote where $\sqrt{\alpha t}/a << 1$ and the thick penetration depth asymptote where $\sqrt{\alpha t}/a >> 1$.

The instantaneous heat transfer rate from the sphere surface into the surroundings is obtained from Fourier's Law of Conduction:

$$Q = k 4\pi a^2 \left( -\frac{\partial \theta}{\partial r} \right)_{r=a} = 4\pi a^2 k \frac{\theta_0}{a} + 4\pi a^2 k \frac{\theta_0}{\sqrt{\pi}\sqrt{\alpha t}}, \quad t > 0 \tag{49}$$

The above expression can be written in terms of two asymptotic heat transfer rates:

$$Q = Q_\infty + Q_0 \tag{50}$$

$$Q = \begin{cases} Q_0 = 4\pi a^2 k \left( \dfrac{\theta_0}{\sqrt{\pi}\sqrt{\alpha t}} \right) & \text{as} \quad \dfrac{\sqrt{\alpha t}}{a} \to 0 \\ Q_\infty = 4\pi a^2 k \left( \dfrac{\theta_0}{a} \right) & \text{as} \quad \dfrac{\sqrt{\alpha t}}{a} \to \infty \end{cases} \tag{51}$$

The solution for the external transient conduction from the surface of an isothermal sphere into a medium of large extent shows a striking resemblance to steady conduction through a spherical wall of thickness $L$ on a sphere of radius $a$. The infinitely thick layer asymptote where $L/a \to \infty$ is identical to the steady-state solution asymptote where $\sqrt{\alpha t}/a \to \infty$.

The layer thickness in the steady conduction problem and the thermal penetration depth in the transient conduction problem play similar roles.

The dimensionless heat transfer rate at the sphere surface is defined as

$$Q^{\star}_{\mathcal{L}} = \frac{Q\mathcal{L}}{Ak\theta_0} \tag{52}$$

where $\mathcal{L}$ represents some arbitrary length scale which is related to the dimensions of the sphere gives

$$Q^{\star}_{\mathcal{L}} = \frac{\mathcal{L}}{a} + \frac{\mathcal{L}}{\sqrt{\pi}\sqrt{\alpha t}} \tag{53}$$

If we choose the recommended length scale [12], i.e. $\mathcal{L} = \sqrt{A}$, we obtain the relationship:

$$Q^{\star}_{\sqrt{A}} = 2\sqrt{\pi} + \frac{1}{\sqrt{\pi}\sqrt{\alpha t/A}} \tag{54}$$

The dimensionless time $\alpha t/A$ is often denoted as $Fo$. Comparison with the general model leads to the following relationships: $\phi = Q^{\star}_{\sqrt{A}}$, $\phi_0 = 1/\sqrt{\pi}\sqrt{Fo}$, $\phi_\infty = 2\sqrt{\pi}$ and $\xi = Fo$. The dimensionless parameters and the corresponding constants and exponents are listed in Table 6. Plots of

TABLE VI
Parameters for Transient Conduction External Isothermal Sphere

| $\phi$ | $\xi$ | $C_0$ | $m$ | $C_\infty$ | $n$ | $p$ |
|---|---|---|---|---|---|---|
| $Q^{\star}_{\sqrt{A}}$ | $Fo$ | $1/\sqrt{\pi}$ | $-1/2$ | $2\sqrt{\pi}$ | 0 | 1 |

the asymptotes show that $\phi_0 > \phi_\infty$ as $\xi \to 0$ and the solution is concave upwards. The model must be as shown in Fig. 2 and Eq. (2) must be used. This is in agreement with the analytical solution.

The first term on the right hand side of the relationship is the dimensionless shape factor $S^{\star}_{\sqrt{A}}$ valid for steady conduction from an isolated isothermal convex body in a medium of large extent. The following general simple compact model with "fitting" parameter $p$ can be used for external transient conduction from arbitrary isothermal convex bodies into a medium of large extent:

$$Q^{\star}_{\sqrt{A}} = \left[ \left( S^{\star}_{\sqrt{A}} \right)^p + \left( \frac{1}{\sqrt{\pi}\sqrt{\alpha t/A}} \right)^p \right]^{1/p} \tag{55}$$

The "fitting" parameter will depend on the body shape and its aspect ratio. This more general simple compact model was used to model transient conduction from the isothermal convex bodies shown in Fig. 7. The figure shows oblate and prolate spheroids, cuboids, the circular and square disks, the rectangular strip, the sphere and the cube. The aspect ratio of the bodies lies in the range: $0 \le AR \le 10$. The numerical values[17] of $Q^{\star}_{\sqrt{A}}$ for the various bodies are shown in Fig. 8 for the wide range: $10^{-6} \le \alpha t/A < 10^3$. All numerical values approach and lie on the asymptote corresponding to very short times and follow the trend of the sphere for $Fo > 10^{-4}$. The values of the dimensionless shape factor lie in the relatively narrow range[17]: $3.19 \le S^{\star}_{\sqrt{A}} \le 4.20$. The "fitting" parameter depends on the aspect ratio, and its values are in the narrow range[17]: $0.87 \le p \le 1.10$. The smaller values of $p$ correspond to bodies with high aspect ratios and the larger values of $p$ correspond to bodies with small aspect ratios.

## VIII. Elastic-Plastic Model for Contact Between Hemisphere and Flat

The mechanical contact between a rigid hemisphere having radius of curvature $\rho$ and a flat substrate with radius of curvature $\rho \to \infty$ is a circular area whose radius is $a$. The elastic properties of the hemisphere and the substrate are Young's modulus: $E_1$ and $E_2$, and Poisson's ratio: $\nu_1$ and $\nu_2$. The subscripts 1 and 2 denote the hemisphere and substrate respectively. The Brinell hardness of the substrate is much smaller than the Brinell hardness of the hemisphere.

If the contact strain defined as $\epsilon_c = a/\rho << 1$, the deformation of the hemisphere and the substrate is elastic, and the classical elasticity theory of Hertz can be used to calculate the magnitude of the contact radius. The Hertz elastic contact model in [18,19] shows that the contact radius is given by the relationship:

$$a_e = \left( \frac{3}{4} \frac{F\rho}{E'} \right)^{1/3} \tag{56}$$

where $F$ is the steady axial mechanical load supported by the contact area, and $E'$ is the effective modulus of the contact [18,19]:

$$\frac{1}{E'} = \frac{1-\nu_1^2}{E_1} + \frac{1-\nu_2^2}{E_2} \tag{57}$$

For a particular contact, the geometry and elastic properties are fixed and the mechanical load is the variable. Therefore, the elastic contact radius relationship can be expressed as

$$a_e = c_e F^{1/3} \qquad \text{where} \quad c_e = \left( \frac{3}{4} \frac{\rho}{E'} \right)^{1/3} \tag{58}$$

This relationship shows how the contact radius increases with the load.

As the load increases, the contact strain increases, and the maximum shear zone which lies on the axis of the contact at points some distance below the contact area, grows in some complex manner [19,20,21]. For very large contact strains, $\epsilon_c < 1$, the deformation of the substrate becomes fully plastic.

The contact radius under these conditions no longer depends on the elastic properties, but does depend on the plastic property of the substrate. The plastic yield is related to the Brinell hardness $H_B$ of the substrate, and its assumed to be a fully work-hardened solid.

From a force balance applied to the contact area we find the relationship for the plastic contact radius [19,21]:

$$a_p = \left( \frac{F}{\pi H_B} \right)^{1/2} \tag{59}$$

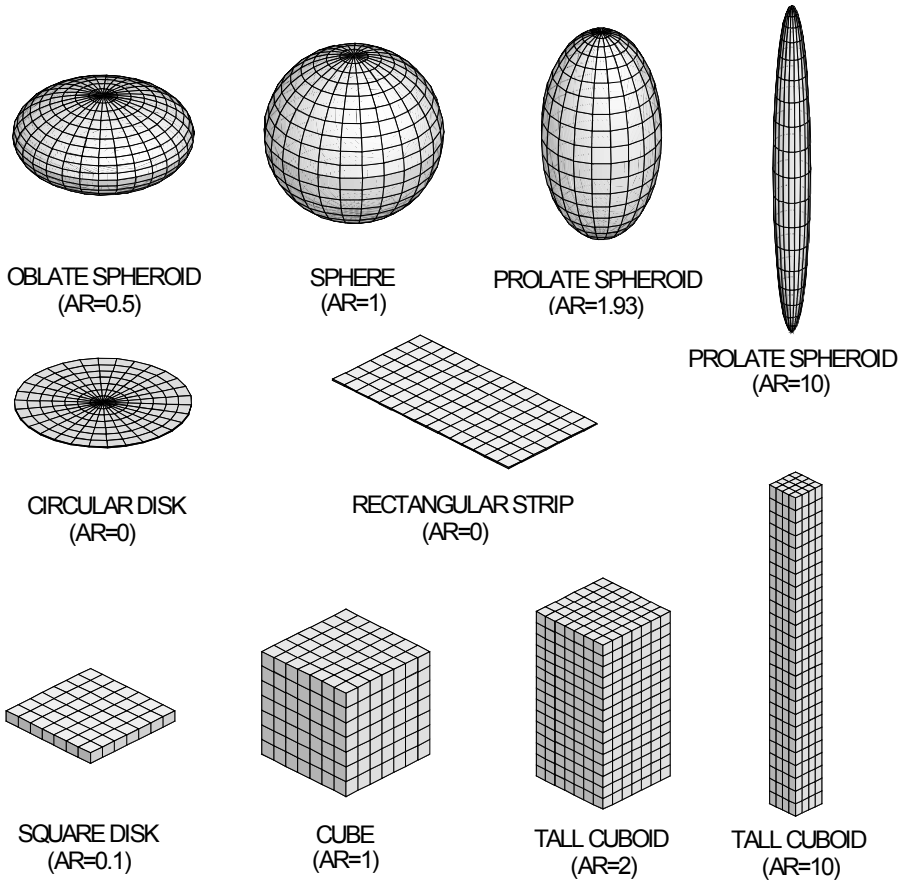


Fig. 7. Ellipsoids and Cuboids for External Transient Conduction

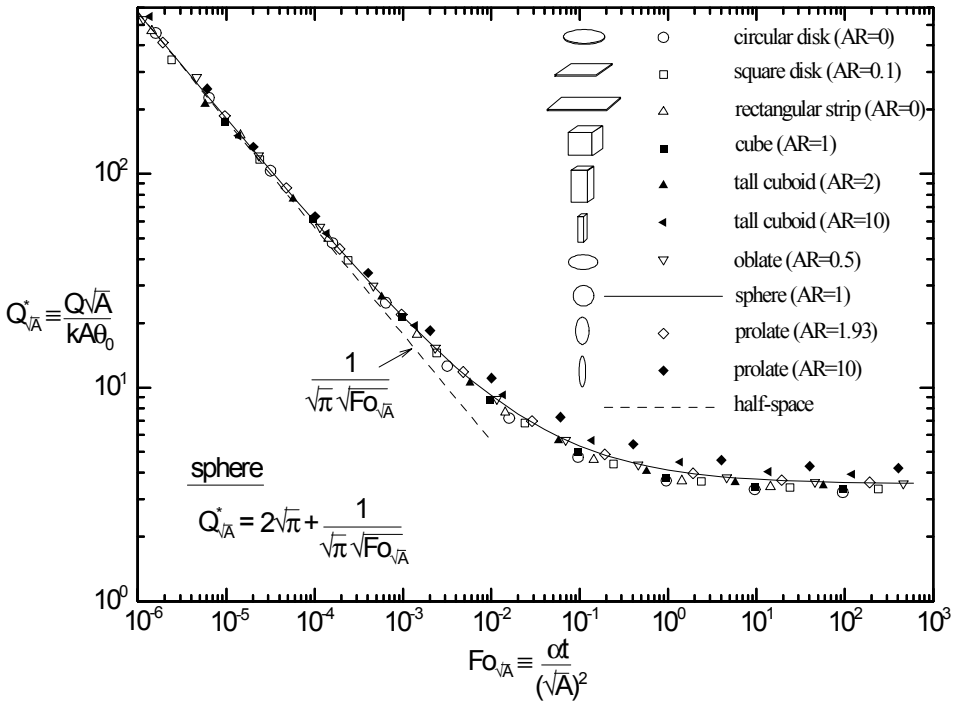


Fig. 8. Comparison of Numerical Values and Compact Model for Transient Conduction from Ellipsoids and Cuboids

This relation can be written as

$$a_p = c_p F^{1/2} \qquad \text{where} \quad c_p = \left(\frac{1}{\pi H_B}\right)^{1/2} \tag{60}$$

which clearly shows how the plastic contact radius grows with the mechanical load. From pure elastic deformation to pure plastic deformation, there is a smooth transition from the elastic contact asymptote to the plastic contact asymptote which are defined as [20]:

$$a = \begin{cases} a_e & \text{for} \quad \epsilon << \epsilon_c \\ a_p & \text{for} \quad \epsilon >> \epsilon_c \end{cases} \tag{61}$$

A model for the elastic-plastic contact can be developed in the following manner. The elastic and plastic contact radii are equal when the mechanical load is $F_c$ [20]

$$a_e = a_p \qquad \text{gives} \quad c_e F_c^{1/3} = c_p F_c^{1/2} \tag{62}$$

Solving for $F_c$ gives the relationship:

$$F_c = \left(\frac{c_e}{c_p}\right)^6 \tag{63}$$

which can be expressed as [20]

$$F_c = \left(\frac{9\pi^3}{16}\right) \rho^2 H_B \left(\frac{H_B}{E'}\right)^2 \tag{64}$$

This equation shows the important relationship between the critical mechanical load $F_c$ and the radius of curvature $\rho$, the elastic properties $E'$ and the Brinell hardness $H_B$.

The critical contact radius $a_c$ can be found from substitution of $F = F_c$ in the relationship for $a_e$ or the relationship for $a_p$. In both cases, the critical contact radius is [20]

$$a_c = \frac{3\pi}{4} \frac{\rho H_B}{E'} \tag{65}$$

The two asymptotes for the contact radius can now be established by defining the relative load on the contact area:

$$\xi = \frac{F}{F_c} \tag{66}$$

The asymptotes for the contact radius are [20]

$$a = \begin{cases} a_e & \text{as} \quad \xi \to 0 \\ a_p & \text{as} \quad \xi \to \infty \end{cases} \tag{67}$$

For practical applications we can say that the contact is elastic provided $\xi < 0.05$, and the contact is plastic provided $\xi > 20$. The elastic-plastic transition lies in the practical interval: $0.05 \le \xi \le 20$. The plots of the elastic and plastic asymptotes show that $a_e > a_p$ as $\xi \to 0$ and the solution is concave upwards in the transition from elastic to plastic deformation. The first model, Eq. (2), must be used for this problem.

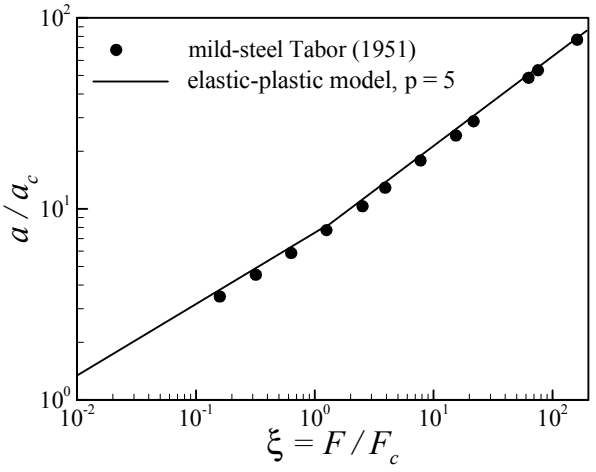


Fig. 9. Comparison of Elastic-Plastic Compact Model and Data for Contact Between Hard Sphere and Mild Steel Substrate

The elastic-plastic transition can be modeled accurately by means of the following simple compact model based on the contact radius [20]:

$$a = \left(a_e^p + a_p^p\right)^{1/p} \qquad \text{with} \quad p = 5 \tag{68}$$

with the "fitting" parameter value $p = 5$ obtained by comparison of the simple compact model predictions and some accurate experimental data [21] for a particular hemisphere-substrate contact.

The above relationship for contact radius leads to the following relationship in terms of the applied load and the elastic and plastic coefficients $c_e$ and $c_p$:

$$a = \left(c_e^5 F^{5/3} + c_p^5 F^{5/2}\right)^{1/5} \tag{69}$$

The plot in Fig. 9 shows the very good agreement between the simple compact model and the experimental data of [21] for a mild steel substrate. The experimental points are seen to fall in the elastic and plastic regions, as well as in the complex elastic-plastic region for which there is no analytical solution. The model and experimental data are plotted as dimensionless contact radius versus the dimensionless contact load.

## IX. Prandtl Number Functions: Forced and Natural Convection from Isothermal Plates

We next consider the local Prandtl number functions for both laminar boundary layer forced and natural convection from isothermal flat plates. In both examples the local Prandtl number function is developed from analytical asymptotes obtained for very small and very large values of the Prandtl number.

### *A. Prandtl Number Function for Forced Convection*

The boundary layer continuity, momentum and energy equations for the forced laminar flow past an isothermal flat plate have been solved for very small and very large

values of the Prandtl number, i.e., $Pr \to 0$ and $Pr \to \infty$. The analytical solutions have the following asymptotes and the value corresponding to $Pr = 1$ [22,23]:

$$\frac{Nu_x}{\sqrt{Re_x}} = \begin{cases} \dfrac{1}{\sqrt{\pi}}\, Pr^{1/2} & \text{as} \quad Pr \to 0 \\ 0.3321 & \text{at} \quad Pr = 1 \\ 0.3387\, Pr^{1/3} & \text{as} \quad Pr \to \infty \end{cases} \tag{70}$$

From these asymptotes we have the following relationships for the dependent and independent dimensionless parameters:

$$\phi = \frac{Nu_x}{\sqrt{Re_x}} \quad \text{and} \quad \xi = Pr \tag{71}$$

where the local Nusselt and Reynolds numbers are defined as

$$Nu_x = \frac{hx}{k} \qquad \text{and} \qquad Re_x = \frac{Ux}{\nu} \tag{72}$$

The constants and the corresponding exponents for forced convection are [22,23]

$$\begin{aligned} C_0 &= 0.5642 \quad \text{and} \quad m = \frac{1}{2} \\ C_\infty &= 0.3387 \quad \text{and} \quad n = \frac{1}{3} \end{aligned} \tag{73}$$

Plots of the two asymptotes with respect to the Prandtl number show that $\phi_0 < \phi_\infty$ as $\xi \to 0$, and the solution is concave downwards. Therefore, the second model, Eq. (3), must be used. The equation for the "fitting" parameter is

$$\frac{1}{0.3321} = \left[ \left( \frac{1}{0.3387} \right)^p + \left( \frac{1}{0.5642} \right)^p \right]^{1/p} \tag{74}$$

By means of computer algebra systems we obtain the value $p = 4.612607$ rounded to 6 decimals. If one uses the approximate value $p_0 = 9/2 = 4.5$, the model for the local Prandtl number function can be expressed as:

$$\frac{Nu_x}{\sqrt{Re_x}} = F(Pr) = \frac{0.3387\, Pr^{1/3}}{\left[1 + (0.0468/Pr)^{3/4}\right]^{2/9}} \tag{75}$$

which is applicable in the range: $0 < Pr < \infty$. This simple relationship gives values of $F(Pr)$ which are in very good agreement with numerical values. The maximum difference is about 1%.

Churchill and Ozoe [24] recommended the following, slightly less accurate, relationship:

$$\frac{Nu_x}{\sqrt{Re_x}} = F(Pr) = \frac{0.3387\, Pr^{1/3}}{\left[1 + (0.0468/Pr)^{2/3}\right]^{1/4}} \tag{76}$$

valid for $0 < Pr < \infty$, and the restrictions: $Re_x < 5 \times 10^5$ and $Pe_x = Re_x Pr > 100$. The maximum difference between the values obtained by means of this relationship and the numerical values is about 3%. This form of the local Prandtl number function appears in most heat transfer texts [13,14]. The average value of the Nusselt number is given by the relationship:

$$\frac{Nu_L}{\sqrt{Re_L}} = 2\, F(Pr) = \frac{0.6674\, Pr^{1/3}}{\left[1 + (0.0468/Pr)^{2/3}\right]^{1/4}} \tag{77}$$

where

$$Nu_L = \frac{hL}{k} \qquad \text{and} \qquad Re_L = \frac{UL}{\nu} \tag{78}$$

The summary of the dimensionless parameters, the constants and the exponents for the local Prandtl number function for forced convection from an isothermal flat plate are listed in Table 6.

TABLE VII
Parameters for Forced Convection Past Isothermal Flat Plate

| $\phi$ | $\xi$ | $C_0$ | $m$ | $C_\infty$ | $n$ | $p$ | $p_0$ |
|---|---|---|---|---|---|---|---|
| $\dfrac{Nu_x}{\sqrt{Re_x}}$ | $Pr$ | 0.564 | 0.5 | 0.338 | 1/3 | 4.613 | 4.5 |

### *B. Prandtl Number Function for Natural Convection*

The laminar boundary layer continuity, momentum and energy equations for the buoyancy-induced laminar flow past a vertical isothermal flat plate have been solved for very small and very large values of the Prandtl number, i.e., $Pr \to 0$ and $Pr \to \infty$. The analytical solutions have the following asymptotes and the value corresponding to $Pr = 1$ [22,23]:

$$\frac{Nu_x}{Ra_x^{1/4}} = \begin{cases} 0.6004\, Pr^{1/4} & \text{for} \quad Pr \to 0 \\ 0.401 & \text{at} \quad Pr = 1 \\ 0.5027 & \text{for} \quad Pr \to \infty \end{cases} \tag{79}$$

where $Nu_x$ is the local Nusselt number and $Ra_x$ is the local Rayleigh number which are defined as

$$Nu_x = \frac{h(x)x}{k} \quad \text{and} \quad Ra_x = \frac{g\beta\theta_w x^3}{\alpha\nu} \tag{80}$$

where $\theta_w = T_w - T_\infty$ is the constant temperature difference at the wall.

From these asymptotes we have the following relationships for the dependent and independent dimensionless parameters:

$$\phi = \frac{Nu_x}{Ra_x^{1/4}} \quad \text{and} \quad \xi = Pr \tag{81}$$

The constants and the corresponding exponents for natural convection are

$$\begin{aligned} C_0 &= 0.6004 \quad \text{and} \quad m = \frac{1}{4} \\ C_\infty &= 0.5027 \quad \text{and} \quad n = 0 \end{aligned} \tag{82}$$

Plots of the two asymptotes with respect to the Prandtl number show that $\phi_0 < \phi_\infty$ as $\xi \to 0$; therefore, the model

given by Eq. (3) must be used. Using the value $\phi = 0.401$ at $\xi_i = 1$, gives the following relationship for the "fitting" parameter $p$:

$$\frac{1}{0.401} = \left[\left(\frac{1}{0.6004}\right)^p + \left(\frac{1}{0.5027}\right)^p\right]^{1/p} \tag{83}$$

Solving for $p$ we obtain the value $p = 2.265478$ rounded to 6 decimals. Churchill and Chu [25] chose the approximate value $p_0 = 9/4 = 2.50$ and recommended the following relationship for the local Prandtl number function:

$$\frac{Nu_x}{Ra_x^{1/4}} = F(Pr) = \frac{0.503}{\left[1 + (0.492/Pr)^{9/16}\right]^{4/9}} \tag{84}$$

which is valid for $0 < Pr < \infty$. This is the function that now appears in most heat transfer texts [13,14].

The Prandtl number function for the mean Nusselt number is defined as

$$\frac{Nu_L}{Ra_L^{1/4}} = \frac{4}{3}F(Pr) = \frac{0.6703}{\left[1 + (0.492/Pr)^{9/16}\right]^{4/9}} \tag{85}$$

with

$$Nu_L = \frac{hL}{k} \quad \text{and} \quad Ra_L = \frac{g\beta\theta_w L^3}{\alpha\nu} \tag{86}$$

where $Nu_L$ is the mean Nusselt number for the plate length $L$.

The summary of the dimensionless parameters, the constants and the exponents for the local Prandtl number function for laminar natural convection from an isothermal flat plate are listed in Table 7.

TABLE VIII
Parameters for Natural Convection Past Vertical Isothermal Flat Plate

| $\phi$ | $\xi$ | $C_0$ | $m$ | $C_\infty$ | $n$ | $p$ | $p_0$ |
|---|---|---|---|---|---|---|---|
| $\dfrac{Nu_x}{Ra_x^{1/4}}$ | $Pr$ | 0.6004 | 1/4 | 0.5027 | 0 | 2.265478 | 2.5 |

The simple compact models for the Prandtl number function for both laminar forced and natural convection from isothermal flat plates can be used to develop other simple compact models such as laminar natural convection heat transfer from isothermal convex bodies of arbitrary shape and aspect ratio. This will be done in the following section.

## X. Laminar Natural Convection from Isothermal Convex Bodies

Laminar natural convection heat transfer from single isothermal convex bodies into a stationary fluid of large extent has been investigated by [26]. A general compact model will be presented next. The simple compact model will be based on two asymptotes corresponding to very small and very large values of the Rayleigh number and the compact model for the Prandtl number function developed above. We seek a general relationship between the dimensionless heat transfer rate $Q^\star_{\mathcal{L}}$ and the Rayleigh number $Ra_{\mathcal{L}}$:

$$Q^\star_{\mathcal{L}} = \frac{Q\mathcal{L}}{Ak\,(T_w - T_\infty)} \qquad Ra_{\mathcal{L}} = \frac{g\beta\,(T_w - T_\infty)}{\alpha\nu}\mathcal{L}^3 \tag{87}$$

where $\mathcal{L}$ denotes the arbitrary length scale of the convex body.

The dimensionless heat transfer rate from the surface of the convex body into its surroundings has the following asymptotes [15,16,27]:

$$Q^\star_{\mathcal{L}} = \begin{cases} S^\star_{\mathcal{L}} & \text{as} \quad Ra_{\mathcal{L}} \to 0 \\ Nu_{\mathcal{L}} & \text{for} \quad 10^4 < Ra_{\mathcal{L}} < 10^{10} \end{cases} \tag{88}$$

where $S^\star_{\mathcal{L}}$ is the dimensionless shape factor for isothermal convex bodies loosing heat by conduction to a stationary medium of large extent, and $Nu_{\mathcal{L}}$ is the laminar thin layer Nusselt number. The Nusselt number is defined as [16,27,28]:

$$Nu_{\mathcal{L}} = F(Pr)\,G_{\mathcal{L}}\,Ra_{\mathcal{L}}^{1/4} \tag{89}$$

It consists of three dimensionless parameters: the area average Prandtl number function $F(Pr)$, the body-gravity function $G_{\mathcal{L}}$ [27,28], and the Rayleigh number $Ra_{\mathcal{L}}$. The Prandtl number function and the body-gravity function are defined and discussed next.

### A. Prandtl Number Function

The Nusselt number depends on the area average Prandtl number function which is defined as [25,27,28]:

$$F(Pr) = \frac{0.670}{\left[1 + (0.5/Pr)^{9/16}\right]^{4/9}} \qquad 0 < Pr < \infty \tag{90}$$

The value of the average Prandtl number function for air is $F(0.71) = 0.515$. Its asymptotic values are $F(Pr \to 0) = 0.800\,Pr^{1/4}$ and $F(Pr \to \infty) = 0.670$. The Prandtl number function is a simple compact model that accounts for the interplay of the thermal and hydrodynamic boundary layers as the hot fluid flows upwards over the convex body.

### B. Body-Gravity Function for Horizontal Cuboids

The body-gravity function is a complex fluid flow parameter that characterizes the manner in which the hot fluid flows over the isothermal convex body under the influence of buoyancy-induced forces. The development of this important dimensionless parameter is given in [27,28]. Although the body-gravity function relationships are known for many body shapes, this presentation will be restricted to the horizontal cuboids shown in Fig. 10. The general cuboid is defined by three lengths: $H, W$ and $L$ as shown in the figure. The length $H$ is parallel to the gravity vector, and the other two lengths define surfaces that are perpendicular to the gravity vector. The four vertical surfaces of the cuboid are defined by the lengths $H, L$ and $H, W$. The

body-gravity function based on $\mathcal{L} = \sqrt{\mathrm{A}}$ where the total wetted cuboid surface area is

$$A = 2\,(HL + HW + LW) \tag{91}$$

is [27]

$$G_{\sqrt{A}} = 2^{1/8}\left[\frac{0.625\,L^{4/3}W + H\,(L+W)^{4/3}}{(HW + HL + LW)^{7/6}}\right]^{3/4} \tag{92}$$

The numerator consists of two terms. The first term is the contribution of the top and bottom horizontal surfaces, and the second term corresponds to the contribution of the vertical side and end surfaces. The denominator is associated with the total surface area of the cuboid.

The calculated values for several cuboids show that they are in the range [27]:

$$0.776 \le G_{\sqrt{A}} \le 1.525 \tag{93}$$

The smallest value corresponds to a horizontal very thin square disk with relative dimensions of $H = 0.01, W = 1, L = 1$. The largest value corresponds to a horizontal very long square bar relative dimensions of $H = 1, W = 1, L = 100$. The value for a horizontal cube is $G_{cube} = 0.985$.

### *C. Dimensionless Shape Factor*

There is no analytical solution for the dimensionless shape factor for an isothermal cuboid. Some numerical values are available that show that $S^{\star}_{\sqrt{A}}$ changes slowly with its shape and the aspect ratios of the sides. For the cube, a numerical value is reported to be $S_{\sqrt{A}} = 3.373$ which compares with the analytical value for the isothermal sphere having the same surface area which is $S^{\star}_{\sqrt{A}} = 2\sqrt{\pi} = 3.545$. The difference is approximately 5%. The numerical values for square cuboids with relative dimensions: $H = 1, W = 1, L = 2, 3, 4, 5$ are $S^{\star}_{\sqrt{A}} = 3.406, 3.465, 3.532, 3.598$, which show the slow change with the aspect ratio. The dimensionless shape factors for isothermal ellipsoids, prolate and oblate spheroids, right circular cylinders and rectangular plates are given in [15].

For this problem we note the dimensionless dependent and independent parameters are $\phi = Q^{\star}_{\sqrt{A}}$ and $\xi = Ra_{\sqrt{A}}$, and the asymptotes are $\phi_0 = S^{\star}_{\sqrt{A}}$ and $\phi_\infty = Nu_{\sqrt{A}}$. Since $\phi_0 > \phi_\infty$ as $\xi \to 0$, the model is concave upwards and the first model given by Eq. (2) must be used. The "fitting" parameter can be found by experimental or numerical methods for some intermediate values of $\xi = Ra_{\sqrt{A}}$. From numerous experiments in air, $Pr = 0.71$, for many different body shapes, its found that $p = 1$ gives acceptable accuracy for the entire range: $0 < Ra_{\sqrt{A}} < 10^{10}$.

### *D. Simple Compact Model for Single Convex Bodies*

The following simple compact model for natural convection from isothermal convex bodies based on $\sqrt{A}$ is recommended for the horizontal cuboids [27]:

$$Q^{\star}_{\sqrt{A}} = S^{\star}_{\sqrt{A}} + F(Pr)\,G_{\sqrt{A}}\,Ra^{1/4}_{\sqrt{A}} \tag{94}$$

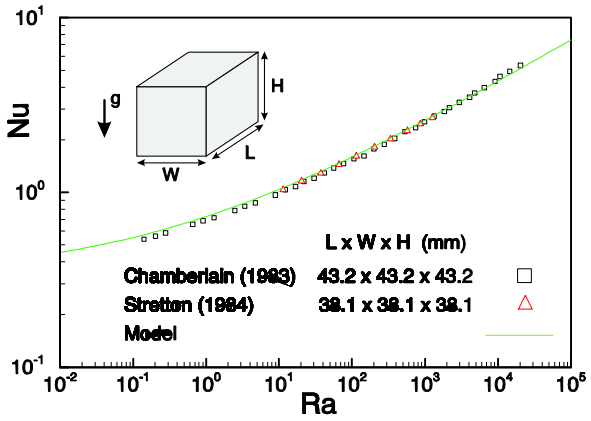


Fig. 11. Compact Model and Air Data for Natural Convection from Cube

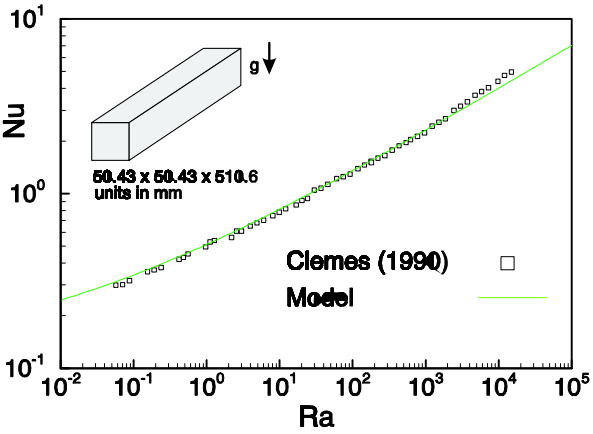


Fig. 12. Compact Model and Air Data for Natural Convection from Horizontal Long Square Cuboid

The model has been compared with air data with many different body shapes over broad ranges of the Rayleigh number and the agreement is very good to excellent. Figures 11 through 13 show comparisons of the simple compact model for air data for the cube, long square cuboid, and the vertical thin cuboids. Figure 14 shows the predictions of the compact model for cuboids and the compact model for natural convection in vertical channels which is not presented in this paper.

## XI. Natural Convection in Vertical Isothermal Ducts and Channels

Convective heat transfer in vertical ducts of arbitrary shape and channels is of great interest to thermal analysts [3, 29]. Although there is interest in models that can handle different wall conditions, this paper will consider the isothermal wall only. It is beyond the scope of this paper to review all the work done by many researchers over several decades [3,29]. The model recently developed [29] will be summarized in this paper. The ducts are characterized by the cross sectional area $A$, its perimeter $P$, and its length $L$. The cross sections of several regular polygo-

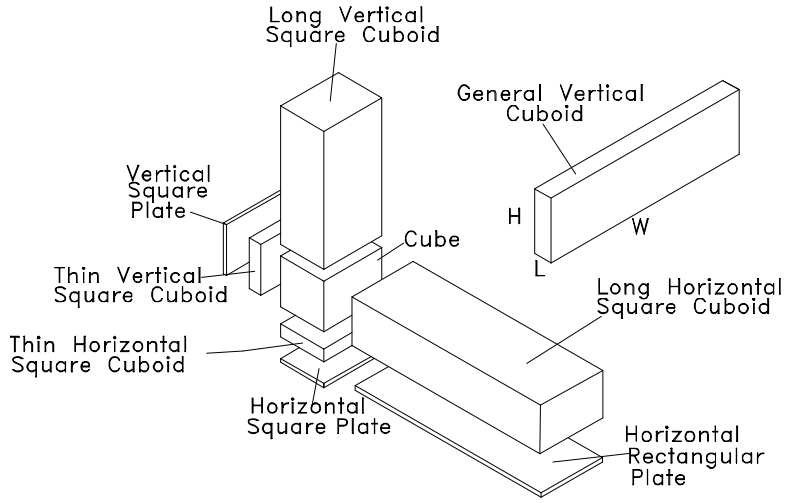


Fig. 10. Schematics of Various Cuboids

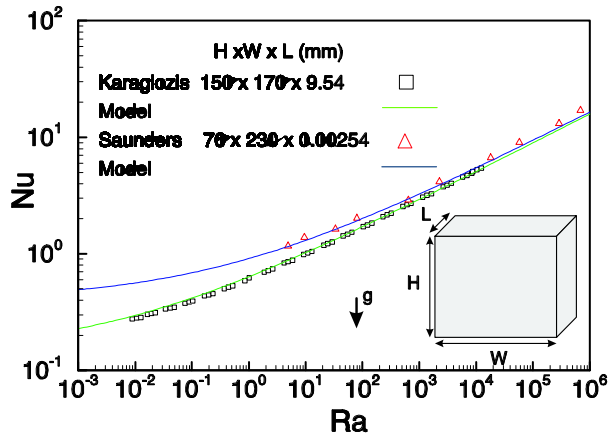


Fig. 13. Compact Model and Air Data for Natural Convection from Vertical Thin Cuboids

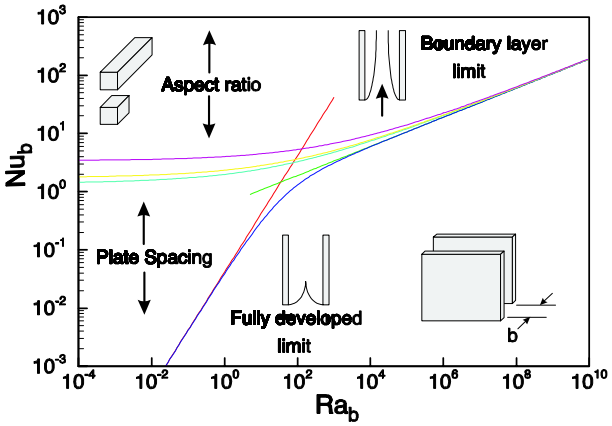


Fig. 14. Compact Models for Cuboids, Parallel Plates, and Heat Sinks

nal ducts, the elliptical duct and the rectangular duct are shown in Fig. 15.

The fluid enters the lower end at some temperature $T_0$ and moves up the duct whose temperature is $T_w > T_0$ due to buoyancy-induced forces. The fluid velocity at the inlet is assumed to be zero.

Its well known from experimental and numerical work that heat transfer from the isothermal wall to the fluid is different when the duct is either very short or when its very long. One criterion for characterizing short and long ducts is to consider the dimensionless geometric parameter:

$$L^\star = \frac{L}{\mathcal{L}} \tag{95}$$

where $\mathcal{L}$ is some characteristic length associated with the duct cross section dimensions. In the past, the hydraulic radius and more frequently the hydraulic diameter $D_h = 4A/P$ have been used to model the convective heat transfer. It can be shown by scaling analysis that there are two asymptotic solutions for this problem which are [29]:

$$Nu_{\mathcal{L}} = \begin{cases} Nu_{bl} & \text{as} \quad L^\star \to 0 \\ Nu_{fd} & \text{as} \quad L^\star \to \infty \end{cases} \tag{96}$$

where $Nu_{bl}$ is called the Nusselt number for boundary layer flow and $Nu_{fd}$ is defined as the Nusselt number for fully-developed flow. The very short duct asymptote is given by following relationship [29]:

$$Nu_{bl} = 0.60\, Ra_L^{1/4} \tag{97}$$

if the duct length $L$ is introduced into the Nusselt and Rayleigh numbers. The relationship becomes [29]:

$$Nu_{bl} = 0.6 \left( Ra_{\sqrt{A}} \frac{\sqrt{A}}{L} \right)^{1/4} \tag{98}$$

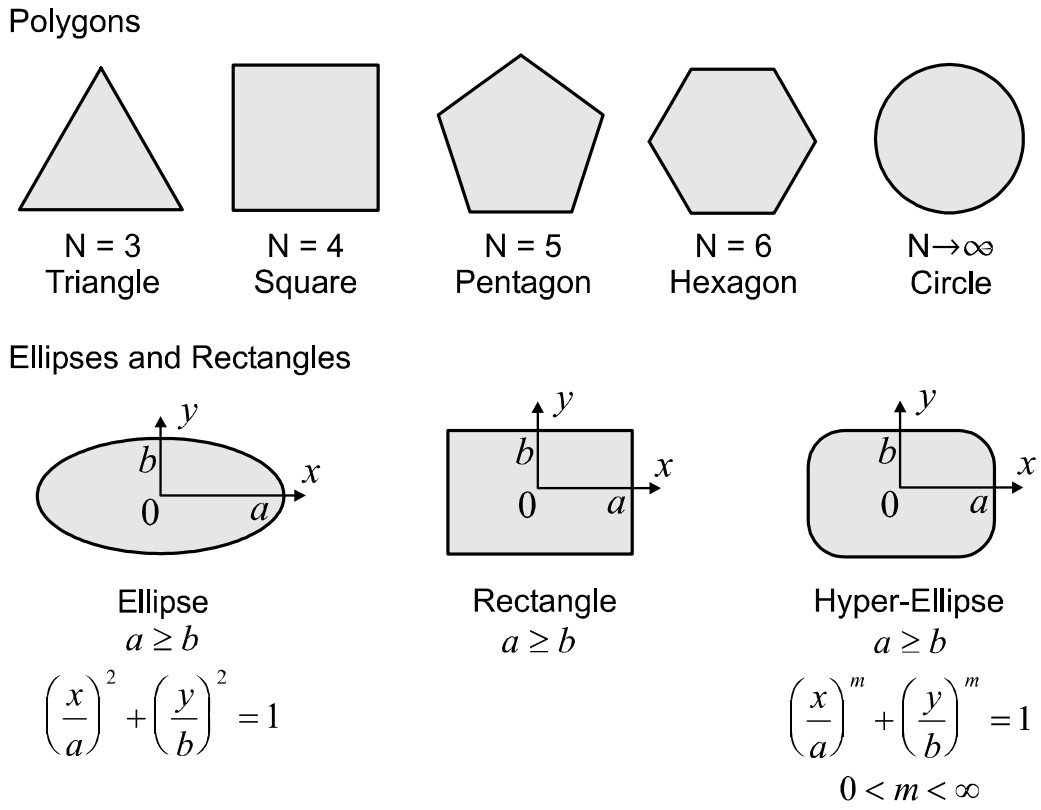


Fig. 15. Cross Sections of Singly Connected Tubes, Pipes and Ducts

when $\mathcal{L} = \sqrt{\mathrm{A}}$ is introduced into both Nusselt and Rayleigh numbers. The geometric parameter $L/\sqrt{A}$ appears which can be used as the criterion for very short and very long ducts. The independent flow parameter [29]:

$$Ra_{\sqrt{A}}\frac{\sqrt{A}}{L} \tag{99}$$

is often called the modified Rayleigh number or the channel Rayleigh number.

The fully-developed flow Nusselt number is given by the following general relationship [29]:

$$Nu_{fd} = \frac{h\mathcal{L}}{k} = 2\frac{Ra_{\mathcal{L}}\dfrac{\mathcal{L}}{L}}{fRe_{\mathcal{L}}}\left(\frac{A}{P\mathcal{L}}\right)^2 \tag{100}$$

when both the Nusselt and Rayleigh numbers are based on the arbitrary length $\mathcal{L}$. If the hydraulic diameter is used, i.e., $\mathcal{L}$ is $D_h$, then we have

$$Nu_{fd} = \frac{Ra_{D_h}\dfrac{D_h}{L}}{8\,fRe_{D_h}} \tag{101}$$

The area average heat transfer coefficient in the Nusselt number is defined as

$$h = \frac{Q}{PL\,(T_w - T_0)} \tag{102}$$

where $Q$ is the total heat transfer rate to the fluid.

If $\mathcal{L}$ is $\sqrt{A}$ in the Nusselt and Rayleigh numbers we obtain the relationship [29]:

$$Nu_{fd} = 2\,\frac{Ra_{\sqrt{A}}\dfrac{\sqrt{A}}{L}}{fRe_{\sqrt{A}}}\left(\frac{\sqrt{A}}{P}\right)^2 \tag{103}$$

The dimensionless relative duct length parameter appears with the Rayleigh number and by itself. Its found to be a very important geometric parameter.

The fluid flow parameter for full-developed flow is $fRe_{\mathcal{L}}$. This parameter is a constant for a particular duct cross section, and it depends only on the duct shape and its aspect ratio. This important parameter is reviewed and discussed in the next section.

We note that $\phi = Nu_{\sqrt{A}}$ and $\xi = Ra_{\sqrt{A}}\sqrt{A}/L$. The asymptotes for very short and very long ducts are

$$\phi_0 = 0.6\,\xi^{1/4} \qquad \text{and} \qquad \phi_\infty = \frac{2}{fRe_{\sqrt{A}}}\left(\frac{\sqrt{A}}{L}\right)^2 \xi \tag{104}$$

and the corresponding constants are, therefore,

$$C_0 = 0.6 \qquad \text{and} \qquad C_\infty = \frac{2}{fRe_{\sqrt{A}}}\left(\frac{\sqrt{A}}{L}\right)^2 \tag{105}$$

For convective heat transfer in a particular duct cross section and fixed length $C_\infty$ = const because the geometric parameter $L/\sqrt{A}$ and $fRe_{\sqrt{A}}$ are constants. Plots of the

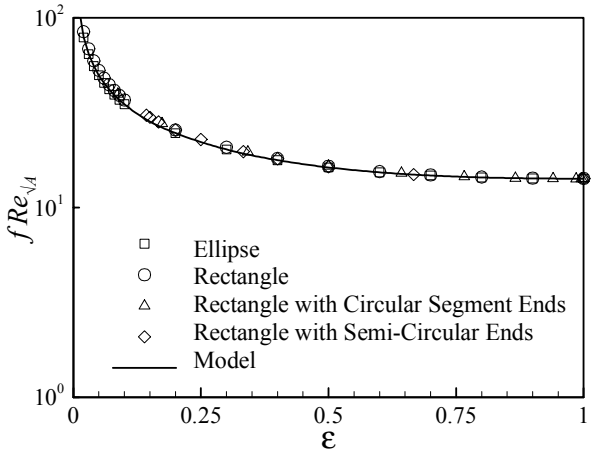


Fig. 16. $fRe$ for Various Duct Cross Sections

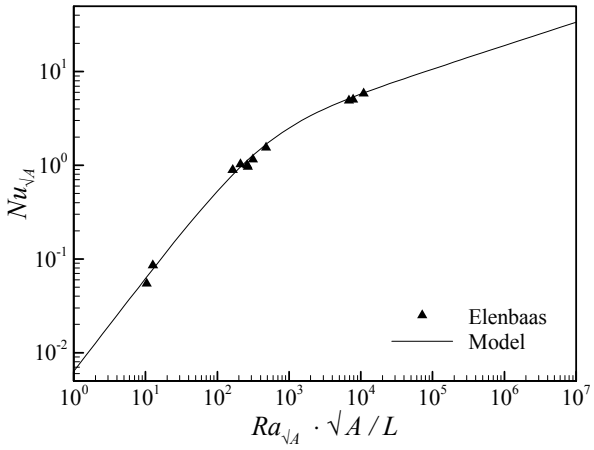


Fig. 17. Compact Model Validation for Triangular Duct

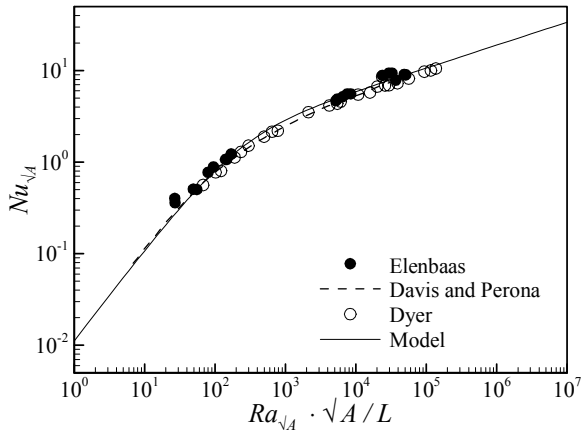


Fig. 18. Compact Model Validation for Circular Duct

two asymptotes show that $\phi_0 < \phi_\infty$ as $\xi \to 0$, therefore the second model given by Eq. (3) must be used. The general compact model for this system is [29]

$$Nu_{\sqrt{A}} = \left\{ \begin{array}{l} \left[0.6\left(Ra_{\sqrt{A}}\frac{\sqrt{A}}{L}\right)^{1/4}\right]^{-p} \\ + \left[2\left(\sqrt{A}/P\right)^2 Ra_{\sqrt{A}}\left(\sqrt{A}/L\right)/fRe_{\sqrt{A}}\right]^{-p} \end{array} \right\}^{-1/p} \quad (106)$$

The compact model was compared against experimental data obtained for air. The polygonal duct shapes such as the equilateral triangle, the square, and the circular duct require the "fitting" parameter to have the value $p = 1.25$ to give small RMS differences.

Comparisons of the compact model predictions against air data for two rectangular ducts having side dimension ratios of 2 and 5 showed that the "fitting" parameter depended on the duct aspect, $\epsilon$ = smaller side/larger side $\leq 1$. The differences between the data and the predicted values are very small when

$$p = \frac{1.2}{\epsilon^{1/9}} \quad (107)$$

It was further demonstrated in [29] that the compact model can be used to predict Nusselt number for the parallel plate channel when the aspect ratio in the model developed for the rectangular duct is set to $\epsilon = 0.01$. The "fitting" parameter for parallel plates channels is $p = 2$.

The fully-developed flow parameter $fRe_{\sqrt{A}}$ developed for the rectangular duct [32,33,35] is shown plotted with respect to $\epsilon$ in Fig. 16. The analytical values for the ellipse, and the numerical values for the rectangular ducts with segment ends and semi-circular ends are seen to be in very close agreement with the curve for the rectangle over the entire range of $\epsilon$.

The compact model and the air data for the equilateral triangle, circle, the rectangle duct with $\epsilon = 0.5$ and the parallel plates channel are shown in Figs. 17 through 20. The agreement between the data and the model predictions is seen to be very good for all duct cross sections.

The recommended compact model can be used to predict natural convection in arbitrary constant cross section ducts provided the cross section does not have sharp corners with small subtended angles.

## XII. Models for Friction Factor Reynolds Number Product

In this example we consider the exact asymptotic model and the approximate models for the friction factor Reynolds product for steady developing and fully-developed laminar flow through constant cross-section pipes of length $L$, cross-sectional area $A$ and perimeter $P$. The fluid enters the pipe with uniform velocity $U$. In the entrance length $0 \leq z \leq L_e$ there are two regions, the core region where the velocity is essentially uniform and increasing with distance from the entrance $z = 0$, and the boundary layer region which lies between the wall and the core region. This very important fluid flow problem is described in [30] and many analytical and numerical results are tabulated in [31] for many different cross sections. New approaches and methods giving new models for singly and

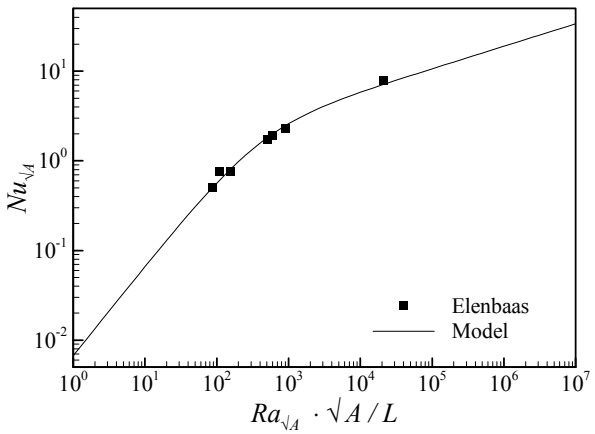


Fig. 19. Compact Model Validation for 2:1 Rectangular Duct

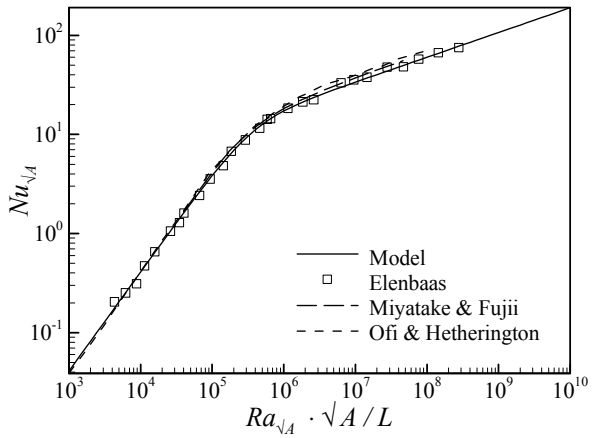


Fig. 20. Compact Model Validation for Parallel Plates Duct

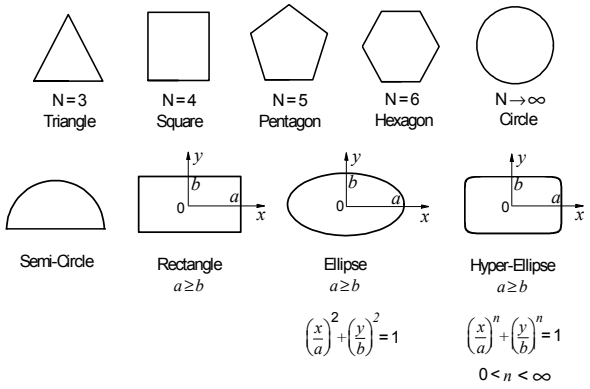


Fig. 21. Common Singly Connected Duct Geometries

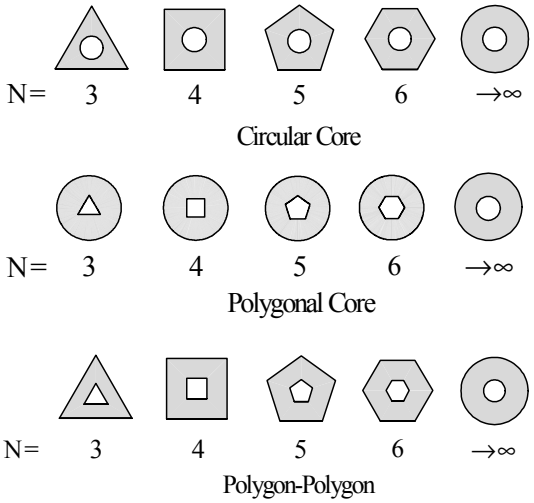


Fig. 22. Doubly Connected Cross Sections

doubly connected cross section tubes, pipes and ducts are presented in [32,33,35]. The new relations to be presented next are capable of predicting pressure drop for fluid flow in the singly connected cross sections shown in Fig. 21, and the doubly connected cross sections shown in Fig. 22.

In the general case the axial fluid velocity depends on axial position $z$ and points in the cross-section, i.e., $w(x, y, z)$. In the core region there is a balance between the pressure and inertia forces, and in the boundary layer region there is a balance between the friction and inertia forces.

In the fully-developed region where $L_e \leq z \leq L$, the fluid velocity no longer depends on distance from the entrance and the fluid velocity depends on points in the cross-section only, i.e., $w(x, y)$, and there is a balance between the pressure and friction forces only.

The local wall shear $\tau_w(x, y, z)$ varies with distance from the pipe entrance and it varies over the perimeter, except for circular pipes and parallel plate channels. There is no analytical solution for the local wall shear for the entire region $0 \leq z \leq L$, even for the relatively simple fluid flows such as flow in a circular pipe or flow between two infinitely large parallel plates, the so-called two-dimensional channel flow. In the two special cases, the local wall shear is constant with respect to the pipe and channel perimeter, however, it varies with distance from the entrance.

Since, in general $\tau_w(x, y, z)$, the average value over the perimeter is defined as

$$\tau_w(z) = \frac{1}{P} \oint_0^P \tau_w(x, y, z) dP \tag{108}$$

where the integration is with respect to points in the perimeter of the pipe.

The overall average value of the wall shear from the pipe entrance to the pipe exit is defined as

$$\tau_w = \frac{1}{L} \int_0^L \tau_w(z) dz \tag{109}$$

The relationship between the overall pressure drop $\Delta p$ and the average wall shear can be obtained from the force balance applied to the entire pipe length, therefore,

$$\Delta p\, A = \tau_w P L \qquad \text{or} \quad \Delta p = \tau_w \frac{PL}{A} \tag{110}$$

The definition of the friction factor-Reynolds number product gives:

$$fRe_{\mathcal{L}} = \left(\frac{2\tau_w}{\rho U^2}\right)\left(\frac{\rho U\mathcal{L}}{\mu}\right) = \frac{2\tau_w\mathcal{L}}{\mu U} = 2\tau_w^\star \tag{111}$$

where $\mathcal{L}$ is some length scale associated with the pipe cross-section. The friction factor and Reynolds number product is related to the dimensionless average wall shear $\tau_w^\star$ with the factor 2.

The relations above can be used to find relations between the pressure drop $\Delta p$ and the mean fluid velocity $U$ or the mass flow rate $\dot{m}$, the geometry of the pipe, the fluid properties, and the friction factor and Reynolds number product. The relations, based on the arbitrary length scale $\mathcal{L}$, are

$$\begin{aligned} \Delta p &= \mu\, U\left(\frac{LP}{A\mathcal{L}}\right)\left(\frac{fRe_{\mathcal{L}}}{2}\right) \\ \Delta p &= \nu\, \dot{m}\left(\frac{LP}{A^2\mathcal{L}}\right)\left(\frac{fRe_{\mathcal{L}}}{2}\right) \end{aligned} \tag{112}$$

The friction factor-Reynolds number product can be obtained by means of scale analyses, asymptotic analyses, and the method of [1] for combining asymptotes.

The scale analyses will be done for very long pipes, i.e., $L/L_e >> 1$ where the fluid flow is fully-developed, and for very short pipes, i.e., $L/L_e << 1$, where the fluid flow is developing in the core and the boundary layer regions. From the scale analyses of [35] the asymptotic relationships are:

$$fRe_{\mathcal{L}} \rightarrow \begin{cases} C_\infty & \text{as} \quad L/L_e \rightarrow \infty \\ \dfrac{C_0}{\sqrt{\xi}} & \text{as} \quad L/L_e \rightarrow 0 \end{cases} \tag{113}$$

where the dimensionless duct length which is based on the arbitrary length scale $\mathcal{L}$ is defined as

$$\xi = \frac{L}{Re_{\mathcal{L}}\mathcal{L}} \tag{114}$$

where $\xi$ depends on the chosen length scale $\mathcal{L}$.

If we let $\phi = fRe_{\mathcal{L}}$, $\phi_0 = C_0$, and $\phi_\infty = C_\infty$, we see that $\phi_0 > \phi_\infty$ as $\xi \rightarrow 0$. Since the trend of $\phi$ with respect to $\xi$ is concave upwards, the asymptotes can be combined in the following manner to give the approximate relationship applicable for all pipe lengths:

$$fRe_{\mathcal{L}} = \left[\left(\frac{C_0}{\sqrt{\xi}}\right)^p + (C_\infty)^p\right]^{1/p} \tag{115}$$

The "fitting" parameter values have been determined for many different pipe cross-sections [32,33,35].

The constant for very short pipes can be found from asymptotic analysis to be $C_0 = 1.72$ for the local value and $C_0 = 3.44$ for the average value of $fRe_{\mathcal{L}}$. These two values are independent of the shape of the pipe cross-section and its aspect ratio.

The constant $C_\infty$ that appears in the very long pipe asymptote depends on the pipe shape, its aspect ratio and the pipe length scale $\mathcal{L}$. These characteristics are clearly seen in the friction factor and Reynolds number product for the rectangular duct whose side dimensions are $2a \times 2b$ with $a \geq b$.

The dimensionless average wall shear was presented in [32,33,35]; and taking the first term of the series solution gives:

$$fRe_{D_h} = \frac{24}{(1+\epsilon^2)\left[1 - \dfrac{192\epsilon}{\pi^5}\tanh\left(\dfrac{\pi}{2\epsilon}\right)\right]} \tag{116}$$

where the duct aspect ratio is defined as $\epsilon = b/a \leq 1$. The duct length scale is based on the hydraulic diameter $D_h$ where

$$D_h = \frac{4A}{P} = \frac{4ab}{a+b} = \frac{4b\epsilon}{1+\epsilon} \tag{117}$$

The relationship based on the hydraulic diameter has two limits which are constants:

$$fRe_{D_h} = \begin{cases} 14.13 & \text{as} \quad \epsilon \rightarrow 1 \\ 24 & \text{as} \quad \epsilon \rightarrow 0 \end{cases} \tag{118}$$

The first limit corresponds to a square duct and the second one corresponds to the parallel plates channel.

When the duct scale length is chosen as $\sqrt{A}$, the relationship becomes

$$fRe_{\sqrt{A}} = \frac{12}{\sqrt{\epsilon}\,(1+\epsilon)\left[1 - \dfrac{192\epsilon}{\pi^5}\tanh\left(\dfrac{\pi}{2\epsilon}\right)\right]} \tag{119}$$

The limits for this relationship are [35]:

$$fRe_{\sqrt{A}} = \begin{cases} 14.13 & \text{as} \quad \epsilon \rightarrow 1 \\ \dfrac{12}{\sqrt{\epsilon}} & \text{as} \quad \epsilon \rightarrow 0 \end{cases} \tag{120}$$

To demonstrate the superiority of $\mathcal{L}$ set to $\sqrt{A}$ in place of $\mathcal{L}$ set to $D_h$ in $fRe_{\mathcal{L}}$, the analytical values for the equilateral triangle, the square and the circle, and the numerical results for the other regular polygonal geometries are listed in Table 9. The aspect ratio for the regular polygonal geometries is $\epsilon \approx 1$. The conversion is

$$fRe_{\sqrt{A}} = \left(\frac{P}{4\sqrt{A}}\right) fRe_{D_h} \tag{121}$$

The values for $fRe_{D_h}$ fall in the range $13.33 \leq fRe_{D_h} \leq 16$ for $3 \leq N \leq \infty$. The relative difference between the triangular and the circular ducts is approximately 16.7 percent. When the characteristic length scale is changed to $\sqrt{A}$, the relative difference is reduced to 7.1 percent for the equilateral triangle, and less than 0.1 percent for the remaining polygons $N \geq 4$. Therefore, the value for the circular duct can be used for all regular polygonal ducts, except the equilateral triangular duct, with negligible errors.

TABLE IX
*fRe* RESULTS FOR REGULAR POLYGONAL GEOMETRIES

| $N$ | $fRe_{D_h}$ | $\frac{fRe^P}{fRe^C}$ | $fRe_{\sqrt{A}}$ | $\frac{fRe^P}{fRe^C}$ |
|---|---|---|---|---|
| 3 | 13.33 | 0.833 | 15.19 | 1.071 |
| 4 | 14.23 | 0.889 | 14.23 | 1.004 |
| 5 | 14.73 | 0.921 | 14.04 | 0.990 |
| 6 | 15.05 | 0.941 | 14.01 | 0.988 |
| 7 | 15.31 | 0.957 | 14.05 | 0.991 |
| 8 | 15.41 | 0.963 | 14.03 | 0.989 |
| 9 | 15.52 | 0.970 | 14.04 | 0.990 |
| 10 | 15.60 | 0.975 | 14.06 | 0.992 |
| 20 | 15.88 | 0.993 | 14.13 | 0.996 |
| $\infty$ | 16 | 1.000 | 14.18 | 1.000 |

Steady laminar fully developed flow of a Newtonian fluid occurs in long elliptical ducts whose semi-axes are $a, b$ with $b \leq a$. The flow is due to a constant pressure gradient $\Delta p/L = -dp/dz$. The analytical closed-form solution of the governing equation has been obtained using elliptic cylinder coordinates. It is

$$w(x,y) = C\left[1 - \frac{x^2}{a^2} - \frac{y^2}{b^2}\right] \tag{122}$$

where

$$C = -\frac{1}{2\mu}\frac{dp}{dz}\frac{a^2b^2}{a^2+b^2} \tag{123}$$

The maximum velocity which occurs on the axis is

$$w_{max} = w(0,0) = C \tag{124}$$

The mean velocity is

$$w_m = \frac{w_{max}}{2} = \frac{C}{2} \tag{125}$$

The velocity distribution can be expressed as

$$\frac{w(x,y)}{w_m} = 2\left[1 - \frac{x^2}{a^2} - \frac{y^2}{b^2}\right] \tag{126}$$

The friction factor can be obtained from the following general relationship:

$$fRe_{\mathcal{L}} = \frac{2}{w_m^\star}\left(\frac{A\mathcal{L}}{b^2 P}\right) \tag{127}$$

where $A$ is the cross section area and $P$ is the perimeter. For the ellipse these geometric parameters are

$$A = \pi ab \qquad P = 4aE(m) \qquad D_h = \frac{4A}{P} = \frac{\pi b}{E(m)} \tag{128}$$

where $E(m)$ is the complete elliptic integral of the second kind of modulus $m = \sqrt{1-\epsilon^2}$, and $\epsilon = b/a \leq 1$. If we choose the hydraulic diameter as the characteristic length, then

$$fRe_{D_h} = 2(1+\epsilon^2)\left[\frac{\pi}{E(m)}\right]^2 \tag{129}$$

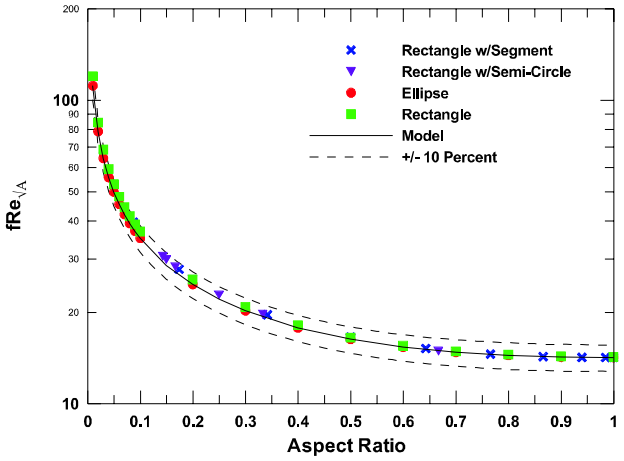


Fig. 23. *fRe* for Fully Developed Flow in Rectangular and Elliptical Ducts

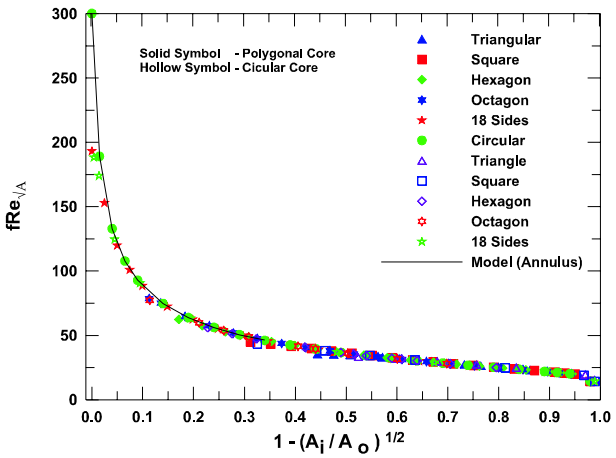


Fig. 24. *fRe* for Fully Developed Flow in Doubly Connected Ducts

If we choose the square root of the cross sectional area, then

$$fRe_{\sqrt{A}} = \frac{2\pi^{3/2}(1+\epsilon^2)}{\sqrt{\epsilon}\,E(m)} \tag{130}$$

The numerical values calculated by means of the two alternative relationships are tabulated in Table 10.

Numerical values for the elliptic and rectangular geometries are presented in Table 10 for both definitions of the characteristic length $\mathcal{L}$ set to $D_h$ and $\sqrt{A}$. Also presented in Table 10 are the ratios of the $fRe$ results for the rectangular duct and the $fRe$ results for the elliptic duct at corresponding aspect ratios. It may be seen from the last column of Table 10, that $\sqrt{A}$ is more appropriate than $D_h$ over the entire range of $\epsilon = b/a$. It is seen that the numerical values for the rectangular and elliptic ducts differ by less than 7% when the characteristic length is $\sqrt{A}$, whereas, if the characteristic length is the hydraulic diameter, the results differ by as much as 31%.

The simple relationship for the rectangular duct with the "fitting" parameter $p = 2$ can be used to obtain approximate numerical values for rectangular ducts with semi-circular ends, elliptical ducts $\epsilon \leq 1$, and the regular polyg-

TABLE X
NUMERICAL VALUES OF $fRe$ FOR ELLIPTICAL AND RECTANGULAR DUCTS

| | $fRe_{D_h}$ | | | $fRe_{\sqrt{A}}$ | | |
|---|---|---|---|---|---|---|
| $\epsilon = b/a$ | Rect. | Ellip. | $\left(\frac{fRe^R}{fRe^E}\right)_{D_h}$ | Rect. | Ellip. | $\left(\frac{fRe^R}{fRe^E}\right)_{\sqrt{A}}$ |
| 0.01 | 23.67 | 19.73 | 1.200 | 119.56 | 111.35 | 1.074 |
| 0.05 | 22.48 | 19.60 | 1.147 | 52.77 | 49.69 | 1.062 |
| 0.10 | 21.17 | 19.31 | 1.096 | 36.82 | 35.01 | 1.052 |
| 0.20 | 19.07 | 18.60 | 1.025 | 25.59 | 24.65 | 1.038 |
| 0.30 | 17.51 | 17.90 | 0.978 | 20.78 | 20.21 | 1.028 |
| 0.40 | 16.37 | 17.29 | 0.947 | 18.12 | 17.75 | 1.021 |
| 0.50 | 15.55 | 16.82 | 0.924 | 16.49 | 16.26 | 1.014 |
| 0.60 | 14.98 | 16.48 | 0.909 | 15.47 | 15.32 | 1.010 |
| 0.70 | 14.61 | 16.24 | 0.900 | 14.84 | 14.74 | 1.007 |
| 0.80 | 14.38 | 16.10 | 0.893 | 14.47 | 14.40 | 1.005 |
| 0.90 | 14.26 | 16.02 | 0.890 | 14.28 | 14.23 | 1.004 |
| 1.00 | 14.23 | 16.00 | 0.889 | 14.23 | 14.18 | 1.004 |

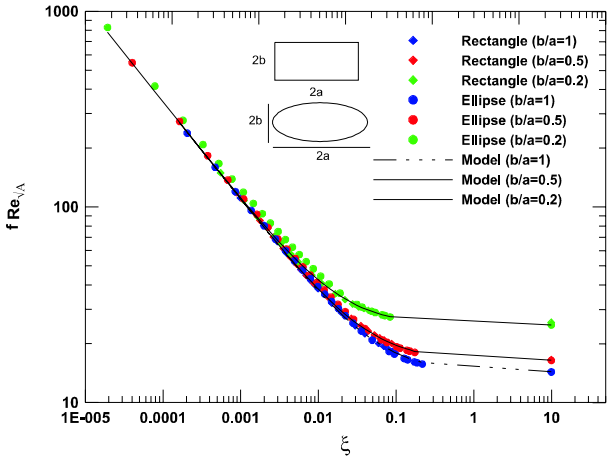


Fig. 25. $fRe$ for Developing Flow in Rectangular and Elliptical Ducts

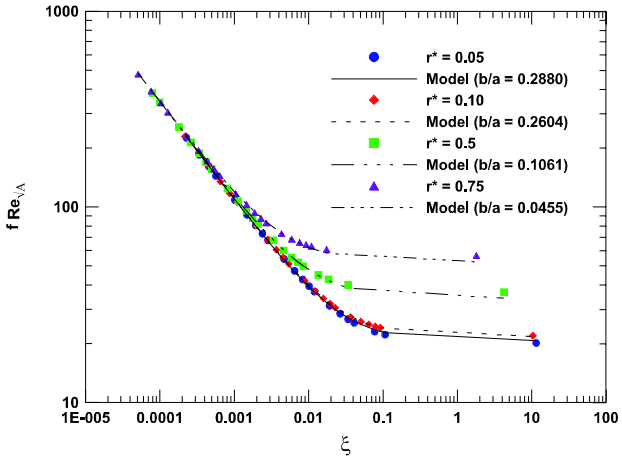


Fig. 27. $fRe$ for Developing Flow in Circular Annular Ducts

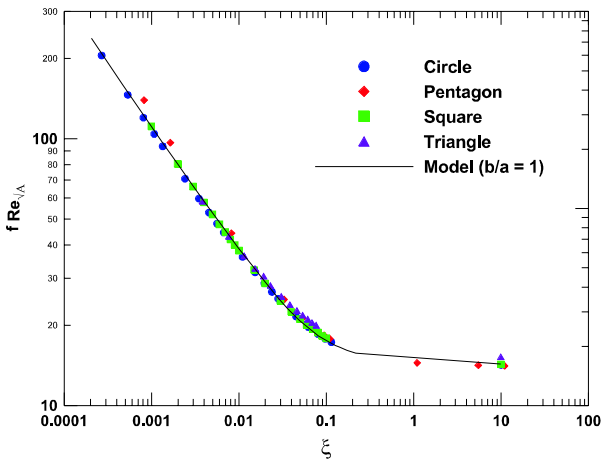


Fig. 26. $fRe$ for Developing Flow in Polygonal Ducts

onal ducts where $\epsilon \approx 1$ and $N \geq 4$.

### A. General Compact Model for Developing Flow

the general compact model for developing flow is given by

$$fRe_{\sqrt{A}} = \left[ \left( \frac{12}{\sqrt{\epsilon}\,(1+\epsilon)\left[1 - \frac{192\epsilon}{\pi^5}\tanh\left(\frac{\pi}{2\epsilon}\right)\right]} \right)^2 + \left(\frac{3.44}{\sqrt{\xi}}\right)^2 \right]^{1/2} \quad (131)$$

TABLE XI
Definitions of Aspect Ratio

| Geometry | Aspect Ratio |
|---|---|
| Regular Polygons | $\epsilon = 1$ |
| Singly-Connected | $\epsilon = \dfrac{b}{a}$ |
| Trapezoid | $\epsilon = \dfrac{2b}{a+c}$ |
| Annular Sector | $\epsilon = \dfrac{1-r^*}{(1+r^*)\Phi}$ |
| Circular Annulus | $\epsilon = \dfrac{(1-r^*)}{\pi(1+r^*)}$ |
| Eccentric Annulus | $\epsilon = \dfrac{(1+e^*)(1-r^*)}{\pi(1+r^*)}$ |

with $p = 2$. The model predictions are compared against numerical values in Figs. 25, 26, and 27. The agreement is seen to be very good for many singly connected ducts shown in Figs. 25 and 26. The very good agreement for circular annular ducts is shown in Fig. 27.

The final results to be considered are those of the circular annulus and other annular ducts which are bounded externally by a polygon or internally by a polygon. It is clear from Fig. 27 that excellent agreement is obtained when the results are re-scaled according to $\sqrt{A}$ and a new aspect ratio defined as $r^* = \sqrt{A_i/A_o}$. This definition was chosen since it returns the same $r^*$ ratio for the circular annular duct. Values for $fRe$ for the circular annulus and other shapes have been examined by [32,32,35].

It should be noted that as the inner boundary approaches the outer boundary, there is some departure from the circular annulus result due to the flow field becoming multiply connected. These points have not been shown on the plot. Limiting values of $r^*$ are provided in [33,33]. It has been found that Eq. (131) may be used to predict values for the circular annulus provided the following equivalent singly connected aspect ratio is defined:

$$\epsilon = \frac{(1-r^*)}{\pi(1+r^*)} \tag{132}$$

This result may be obtained from two different physical arguments. The first is the ratio of the of gap, $r_o - r_i$, to the mean perimeter, while the second is obtained as the ratio of the gap to the equivalent length if the duct area, $\pi(r_o^2 - r_i^2)$, is converted to a rectangle. Both points of view yield the same definition.

It is now clear that Eq. (131) fully characterizes the flow in the long duct limit. The maximum deviation of exact values is of the order 7-10 percent. It has now been shown that the dimensionless average wall shear, $fRe$, may be predicted from Eq. (131), provided an appropriate definition of the aspect ratio is chosen.

## XIII. Forced Convection Heat Transfer in Tubes, Pipes, Ducts and Channels

Convective heat transfer in short and long tubes, pipes, ducts and parallel plates channels is of great importance to thermal analysts. These systems can be characterized by the cross sectional area $A$, perimeter $P$, and the length $L$. The cross sections can be singly or doubly connected as shown in Figs. 21 and 22. If the systems are doubly connected, then there are two perimeters: $P_i, P_o$, the inner and outer perimeters, and two projected areas: $A_i, A_o$, the inner and outer projected areas. The flow area is $A = A_o - A_i$.

The walls can be isothermal or have a uniform heat flux imposed. The fluid is a single phase substance which may be a gas, generally air, or some fluid such as water, oil, or a water-glycol mixture, for example. The local or area-average Nusselt is required for heat transfer calculations. The fluid is assumed to enter one end of the tube with a uniform temperature $T_0$ and a uniform velocity $U$. As the fluid is transported along the tube, a hydrodynamic and a thermal boundary layer develops and they both grow until they occupy the entire cross section. The entrance length for the hydrodynamic boundary layer is denoted as $L_h$ and the entry length for the thermal boundary is denoted as $L_t$.

The asymptotic solutions for thermally fully developed flow, $L >> L_h, L >> L_t$, thermally developing flow, $L >> L_h, L << L_t$, and the combined entry problem, $L << L_h, L << L_t$, will be used to develop a general model for predicting heat transfer coefficients in non-circular ducts.

The details of the development of the relationships are given in some books and handbooks. In this section the results of the analyses done by [32,34,36] will be reported. The scale analyses results [36] for the Nusselt number $Nu_{\mathcal{L}}$ are summarized as

$$Nu_{\mathcal{L}} = \begin{cases} B_1 & L >> L_t, L_h \\ B_2 \left( \dfrac{fRe_{\mathcal{L}}}{L^*} \right)^{1/3} & L << L_t, L >> L_h \\ \dfrac{B_3}{(L^*)^{1/2}} & L << L_t, L_h, \Delta >> \delta \\ \dfrac{B_4}{Pr^{1/6}(L^*)^{1/2}} & L << L_t, L_h, \Delta << \delta \end{cases} \tag{133}$$

The Reynolds number $Re_{\mathcal{L}} = U\mathcal{L}/\nu$ and the Nusselt number $kNu_{\mathcal{L}} = h\mathcal{L}$ are both based on the arbitrary length scale $\mathcal{L}$ which is related to the dimensions of the tube cross section.

There are four asymptotes corresponding to the very short tubes $L << L_h, L << L_t$ and very long tubes where $L >> L_h$, $L_t$. The hydrodynamic and thermal boundary thicknesses are denoted as $\delta$ and $\Delta$, respectively. where $Pr$ $L^* Re_{\mathcal{L}} = L/\mathcal{L}$ is the dimensionless thermal entry length.

*A. Long Tube Asymptote*

By means of asymptotic analysis [36], the very long tube $L >> L_h$, $L >> L_t$ asymptote can be expressed as

$$Nu_{\sqrt{A}} = C_1 \left( \frac{fRe_{\sqrt{A}}}{8\sqrt{\pi}\epsilon^{\gamma}} \right) \tag{134}$$

where $C_1$ is equal to 3.01 for the UWT boundary condition and 3.66 for the UWF boundary condition. These results are the average value for fully developed flow in a polygonal tube when the characteristic length scale is the square root of cross-sectional area [32,34,36]. The cross section aspect ratio is defined as $\epsilon$ = short side/longer side $\leq 1$.

The parameter $\gamma$ is chosen based upon the geometry. Values for $\gamma$ which define the upper and lower bounds are fixed at $\gamma = 1/10$ and $\gamma = -3/10$, respectively. Almost all of the available data are predicted within $\pm$ 10 percent by Eq. (134), with few exceptions.

By means of another asymptotic analysis [36] for short tubes where $L << L_t$ and $L >> L_h$ leads to the following relationship for the Nusselt number:

$$Nu_{\mathcal{L}} = C_2 C_3 \left( \frac{fRe_{\mathcal{L}}}{L^{\star}} \right)^{1/3} \tag{135}$$

where $C_2$ is 1 for local conditions and 3/2 for average conditions, and $C_3$ takes a value of 0.427 for UWT and 0.517 for UWF conditions respectively. The friction factor and Reynolds number product was discussed in an earlier section. The results from that section can be used here.

*B. Short Tube Asymptote*

By means of asymptotic analyses [36] for very short tubes where $L << L_t$ and $L << L_h$ in which both boundary layers are developing simultaneously, the local Nusselt numbers are related to the Reynolds and Prandtl numbers in the following way:

$$\frac{Nu_z}{\sqrt{Re_z}} = \begin{cases} 0.564Pr^{1/2} & Pr \to 0 \\ 0.339Pr^{1/3} & Pr \to \infty \end{cases} \tag{136}$$

for the UWT condition, and

$$\frac{Nu_z}{\sqrt{Re_z}} = \begin{cases} 0.886Pr^{1/2} & Pr \to 0 \\ 0.464Pr^{1/3} & Pr \to \infty \end{cases} \tag{137}$$

for the UWF condition. The asymptotic relationships for the Prandtl number function can be combined into a simple compact relationship given by the following general form:

$$\frac{Nu_z}{(Re_z Pr)^{1/2}} = \frac{C_o}{\left[ 1 + \left( \frac{C_o Pr^{1/6}}{C_\infty} \right)^n \right]^{1/n}} = f(Pr) \tag{138}$$

The average Nusselt number for both cases is now obtained by integrating Eq. (138):

$$\overline{Nu}_{\mathcal{L}} = 2Nu_{\mathcal{L}} \tag{139}$$

After introducing $L^{\star}$, the solution for each wall condition can be compactly written as:

$$Nu_{\mathcal{L}} = C_4 \frac{f(Pr)}{\sqrt{L^{\star}}} \tag{140}$$

where the value of $C_4 = 1$ for local conditions and $C_4 = 2$ for average conditions, and $f(Pr)$ is defined as:

$$f(Pr) = \frac{0.564}{\left[ 1 + \left( 1.664Pr^{1/6} \right)^{9/2} \right]^{2/9}} \tag{141}$$

for the UWT condition, and

$$f(Pr) = \frac{0.886}{\left[ 1 + \left( 1.909Pr^{1/6} \right)^{9/2} \right]^{2/9}} \tag{142}$$

for the UWF condition. The preceding results are valid only for small values of $L^{\star}$.

*C. First Compact Model for Nusselt Number*

The first compact model can be developed for the entire range of dimensionless tube lengths and for $Pr \to \infty$. Its general form is [36]:

$$Nu(z^{\star}) = \left( \left\{ C_2 C_3 \left( \frac{fRe}{z^{\star}} \right)^{\frac{1}{3}} \right\}^n + (Nu_{fd})^n \right)^{1/n} \tag{143}$$

Now using the result for the fully developed friction factor and the result for the fully developed flow Nusselt number with $n \approx 5$, a new model [32,34,36] was proposed having the form:

$$Nu_{\sqrt{A}}(L^{\star}) = \left[ \left\{ C_2 C_3 \left( \frac{fRe_{\sqrt{A}}}{L^{\star}} \right)^{\frac{1}{3}} \right\}^5 + \left\{ C_1 \left( \frac{fRe_{\sqrt{A}}}{8\sqrt{\pi}\epsilon^{\gamma}} \right) \right\}^5 \right]^{\frac{1}{5}} \tag{144}$$

where the constants $C_1$, $C_2$, $C_3$ and $\gamma$ are given in Table 12. These constants define the various cases for local or average Nusselt number and isothermal or isoflux boundary conditions for the Graetz problem. The constant $C_2$ was modified from that found by the Leveque approximation to provide better agreement with the data.

*D. Second Compact Model*

A model for the combined entrance region is now developed by combining the solution for a flat plate with the model for the Graetz flow problem developed earlier. The proposed model takes the form:

$$Nu_{\sqrt{A}}(L^{\star}, Pr) = \left[ \left( \left\{ C_2 C_3 \left( \frac{fRe_{\sqrt{A}}}{L^{\star}} \right)^{\frac{1}{3}} \right\}^5 + \right. \right.$$

$$\left\{C_1\left(\frac{fRe_{\sqrt{A}}}{8\sqrt{\pi}\epsilon^{\gamma}}\right)\right\}^5\Bigg)^{m/5} + \left\{C_4\frac{f(Pr)}{\sqrt{L^\star}}\right\}^m\Bigg]^{1/m} \quad (145)$$

which is similar to that proposed by Churchill and Ozoe [3,4] for the circular duct. This model is a composite solution of the three asymptotic solutions just presented. The "fitting" parameter was found to depend on the Prandtl number [25].

The parameter $m$ was determined to lie in the range $2 < m < 7$, for all data examined. Values for the blending parameter were found to be weak functions of the duct aspect ratio and whether a local or average Nusselt number was considered. However, the blending parameter was found to be most dependent upon the fluid Prandtl number.

A simple linear approximation was determined to provide better accuracy than choosing a single value for all duct shapes. Due to the variation in geometries and data, higher order approximations offered no additional advantage. Therefore, the linear approximation which predicts the blending parameter within 30 percent was found to be satisfactory. Variations in the blending parameter of this order will lead to small errors in the model predictions, whereas variations on the order of 100 percent or more, i.e. choosing a fixed value, produce significantly larger errors. The resulting fit for the correlation parameter $m$ is:

$$m = 2.27 + 1.65Pr^{1/3} \quad (146)$$

The above model is valid for $0.1 < Pr < \infty$ which is typical for most low Reynolds number flow heat exchanger applications.

The compact model predictions and numerical values have been compared [32,34,36] for many duct cross sections (singly and doubly connected), for UWT and Isoflux conditions for area average Nusselt numbers for different fluids characterized by several values of $Pr$. The general compact model, Eq. (145), and numerical values are compared in Figs. 28 through 33 for singly and doubly connected ducts for uniform wall temperature (UWT) and uniform wall flux (UWF). The numerical values for parallel plate channels are compared with the model in Fig. 33. In all cases the agreement is good. Its beyond the scope of this paper to show all plots given in [32,34,36]. A few selected plots are presented to show the good agreement between the compact model predictions and the numerical data tabulated in [31].

## XIV. Summary and Conclusions

Asymptotes appear in many problems in fluid mechanics, contact mechanics, steady and transient conduction and convective heat transfer, as well as many other important thermophysical problems. Often the asymptotes appear explicitly from asymptotic analysis, and other times one of the asymptotes does not appear until a change has been made in the presentation of the analysis.

The method of combining asymptotes is based the work of Churchill and Usagi [1]. It was shown that there are

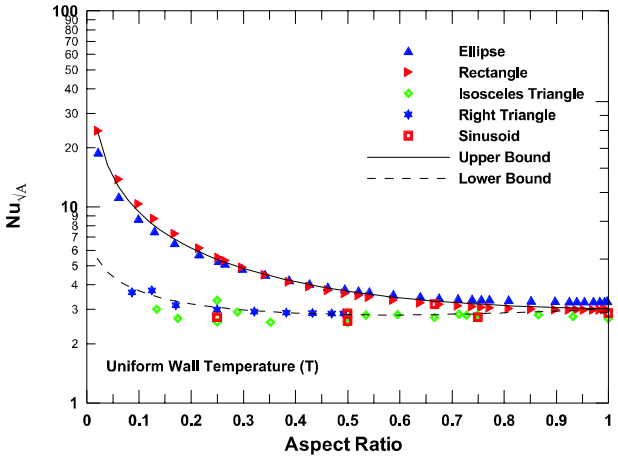


Fig. 28. Nusselt Number for Fully Developed Flow in Various UWT Ducts

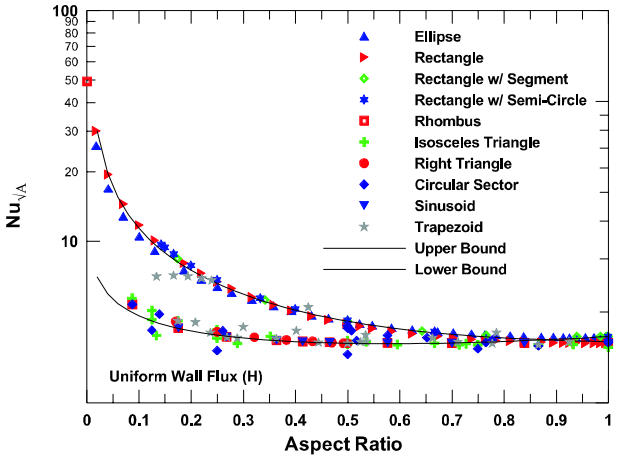


Fig. 29. Nusselt Number for Fully Developed Flow in Various UWF Ducts

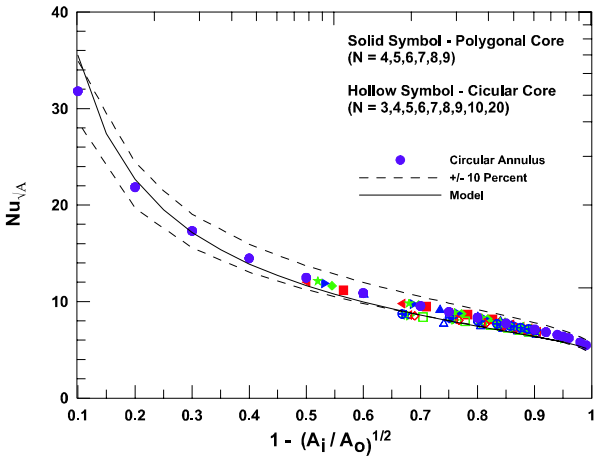


Fig. 30. Nusselt Number for Fully Developed Flow in UWF Annular Ducts

TABLE XII
COEFFICIENTS FOR GENERAL MODEL

| Boundary Condition | | | |
|---|---|---|---|
| UWT (T) | $C_1 = 3.01,\ C_3 = 0.409$ | $f(Pr) = \dfrac{0.564}{\left[1 + \left(1.664 Pr^{1/6}\right)^{9/2}\right]^{2/9}}$ | |
| UWF (H) | $C_1 = 3.66,\ C_3 = 0.501$ | $f(Pr) = \dfrac{0.886}{\left[1 + \left(1.909 Pr^{1/6}\right)^{9/2}\right]^{2/9}}$ | |
| **Nusselt Number Type** | | | |
| Local | $C_2 = 1$ | $C_4 = 1$ | |
| Average | $C_2 = 3/2$ | $C_4 = 2$ | |
| **Shape Parameter** | | | |
| Upper Bound | $\gamma = 1/10$ | | |
| Lower Bound | $\gamma = -3/10$ | | |

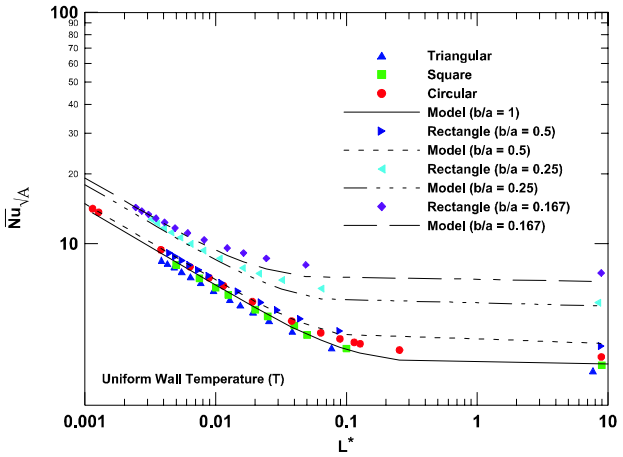


Fig. 31. Nusselt Number for Thermally Developing Flow in Various UWT Ducts

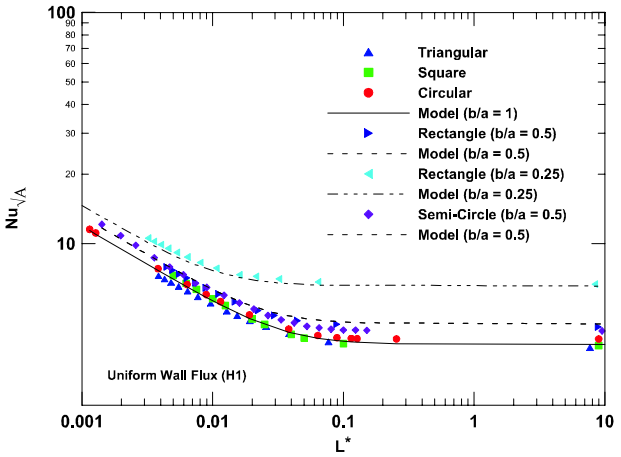


Fig. 32. Nusselt Number for Thermally Developing Flow in Various UWF Ducts

two basic ways of combining the asymptotes depending on where the approximate solution is concave upwards or concave downwards. A procedure of calculating the "fitting" parameter was presented. The approximate solutions for many different types of problems were shown to be very accurate over broad ranges of the independent parameters.

The examples presented include conduction through a stationary gas for all values of the Knudsen number, radiation through a porous layer of material, steady conduction through a spherical wall and enclosures with constant gap thickness, transient conduction external to a sphere and other convex bodies, elastic-plastic contact of a rigid sphere and a softer substrate, pressure drop for fluid flow through short and long tubes of arbitrary cross sectional area, natural convection in vertical isothermal ducts of arbitrary cross sectional area, and finally forced convection heat transfer in short and long tubes and pipes with isothermal and isoflux wall conditions. The last example showed how several asymptotes can be combined to develop a compact model.

Many of the examples have previously been applied to some interesting microelectronics cooling problems.

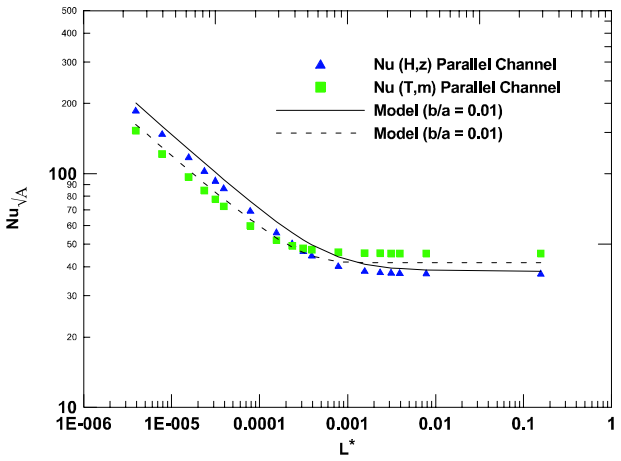


Fig. 33. Nusselt Number for Thermally Developing Flow in Parallel Plate Channels

## XV. Acknowledgments

The continued support of the Natural Sciences and Engineering Research Council of Canada, NSERC, and funding from Manufacturing and Materials of Ontario, MMO, are greatly appreciated. The assistance of M. Bahrami, W. Khan, P. Teerstra, Y. Muzychka, and R. Culham in the preparation of this Keynote paper is also greatly appreciated.

## XVI. References

1. Churchill, S.W. and Usagi, R., (1972), "A General Expression for the Correlation of Rates of Transfer and Other Phenomena", *American Institute of Chemical Engineers*, Vol. 18, pp. 1121-1128.
2. Churchill, S.W., (1988). *Viscous Flows: The Practical Use of Theory*, Butterworths, Boston, MA.
3. Kraus, A.D. and Bar-Cohen, A., (1983). *Thermal Analysis and Control of Electronic Equipment*, Hemisphere Publishing Corporation, New York, NY.
4. Muzychka, Y.S. and Yovanovich, M.M., (2001). "Thermal Resistance Models for Non-Circular Moving Heat Sources on a Half Space," *Journal of Heat Transfer*, Vol. 123, August, pp. 624-632.
5. Song, S. (1988). "Analytical and Experimental Study of Heat Transfer Through Gas Layers of Contact Interfaces," Ph.D. Thesis, University of Waterloo, Canada.
6. Song, S., Yovanovich, M.M., and Goodman, F.O. (1993). "Thermal Gap Conductance of Conforming Rough Surfaces in Contact," *J. Heat Transfer*, Vol. 115, pp. 533-540.
7. Hartnett, J.P., (1961). "A Survey of Thermal Accommodation Coefficients," Rarefied Gas Dynamics, L. Talbot, ed., Academic Press, pp. 1-28.
8. Wachman, H.Y., (1962). "The Thermal Accommodation Coefficient: A Critical Survey," Amer. Rocket Soc. J., Vol. 32, pp. 2-12.
9. Teagan, W.P., and Springer, G.S. (1968). "Heat Transfer and Density-Distribution and Measurements Between Parallel Plates in the Transition Regime," *Physics of Fluids*, Vol. 11, No. 3, pp. 497-506.
10. Braun, D., and Frohn, A. (1977). "Heat Transfer in Binary Mixtures of Monatomic Gases for High-Temperature Differences and for a Large Knudsen Number Range," *Rarefied Gas Dynamics*, J.L. Potter, ed., pp. 149-159.
11. Gebhart, B., (1971). *Heat Transfer*, Second Edition, McGraw-Hill, New York, NY, pp. 165-167.
12. Carslaw, H.S., and Jaeger, J.C. (1959). *Conduction of Heat in Solids*, 2nd ed., Oxford Press, London.
13. Incropera, F.P. and DeWitt, D.P., (1990). *Fundamentals of Heat and Mass Transfer*, Wiley, New York, NY.
14. Bejan, A., (1993). *Heat Transfer*, Wiley, New York, NY.
15. Yovanovich, M.M. (1995). "Dimensionless Shape Factors and Diffusion Lengths of Three Dimensional Bodies," 4th ASME/JSME Thermal Engineering Joint Conference, Lahaina, Maui, HI, March 19-24.
16. Yovanovich, M. M., (1987). "New Nusselt and Sherwood Numbers for Arbitrary Isopotential Bodies at Near Zero Peclet and Rayleigh Numbers," AIAA 87-1643, AIAA 22nd Thermophysics Conference, Honolulu, Hawaii, June 8-10.
17. Yovanovich, M.M., Teertstra, P.M., and Culham, J.R., (1995). "Modeling Transient Conduction from Isothermal Convex Bodies of Arbitrary Shape", *Journal of Thermophysics and Heat Transfer*, Vol. 9, pp. 385-390.
18. Timoshenko, S.P., and Goodier, J.N. (1970). *Theory of Elasticity*, 3d ed. McGraw-Hill, New York, NY.
19. Johnson, K.L. (1985). *Contact Mechanics*, Cambridge University Press, Cambridge.
20. Sridhar, M.R., and Yovanovich, M.M. (1996). "Elastoplastic Constriction Resistance Model for Sphere-Flat Contacts," *J. of Heat Transfer*, Vol. 118, No. 1, February, pp. 202-205.
21. Tabor, D. (1951). *The Hardness of Metals*, Oxford University Press, London.
22. Kays, W.M., and Crawford, M.E., (1993). *Convective Heat and Mass Transfer*, McGraw-Hill, New York.
23. Bejan, A., (1995). *Convection Heat Transfer*, $2^{nd}$ Edition, Wiley, New York, NY.
24. Churchill, S.W. and Ozoe, H., (1973). "Correlations for Laminar Forced Convection in Flow Over an Isothermal Flat Plate and in Developing and Fully Developed Flow in an Isothermal Tube," *J. of Heat Transfer*, Vol. 95, pp. 416-419.
25. Churchill, S.W. and Chu, H.H.S., (1975). "Correlating Equations for Laminar and Turbulent Free Convection from a Vertical Plate," *Int. J. Heat Mass Transfer*, Vol. 18, p. 1323.
26. Hassani, A, (1987). "An Investigation of Free Convection Heat Transfer from Bodies of Arbitrary Shape," Ph.D. Thesis, University of Waterloo.
27. Yovanovich, M.M. and Jafarpur, K. (1993). "Models of Laminar Natural Convection from Vertical and Horizontal Isothermal Cuboids for All Prandtl Numbers and Rayleigh Numbers Below $10^{11}$," 114th ASME Winter Annual Meeting, New Orleans, LA, November 28-December 3.
28. Lee, S., Yovanovich, M.M., and Jafarpur, K. (1991).

"Effects of Geometry and Orientation on Laminar Natural Convection from Isothermal Bodies," *J. Thermophysics*, Vol. 5, No. 2, pp. 208-216.
29. M.M. Yovanovich, P. Teertstra, and Y.S. Muzychka, (2002). "Natural Convection Inside Vertical Isothermal Ducts of Constant Arbitrary Cross-Section", *Journal of Thermophysics and Heat Transfer*, Vol. 16, No. 1, January-March, pp. 116-121.
30. Knudsen, J.G. and Katz, D.L., (1958). *Fluid Dynamics and Heat Transfer*, McGraw-Hill, New York, NY.
31. Shah, R.K. and London, A.L., ( 1978). *Laminar Flow Forced Convection in Ducts*, Academic Press, New York, NY.
32. Muzychka, Y.S., (1999). *Analytical and Experimental Study of Fluid Friction and Heat Transfer in Low Reynolds Number Flow Heat Exchangers*, Ph.D. Thesis, University of Waterloo, Waterloo, ON.
33. Muzychka, Y.S. and Yovanovich, M.M., (1998). "Modeling Fricton Factors in Non-Circular Ducts for Developing Laminar Flow," AIAA 98-2492, 2nd Theoretical Fluid Mechanics Meeting, Albuquerque, NM.
34. Muzychka, Y.S. and Yovanovich, M.M., (1998). "Modeling Nusselt Numbers for Thermally Developing Laminar Flow in Non-Circular Ducts," AIAA 98-2586, 7th AIAA/ASME Joint Thermophysics and Heat Transfer Conference, Albuquerque, NM.
35. Muzychka, Y.S. and Yovanovich, M.M., (2002). "Laminar Flow Friction and Heat Transfer in Non-Circular Ducts and Channels: Part I - Hydrodynamic Problem," *Compact Heat Exchangers*, A Festschrift on the $60^{th}$ Birthday of Ramesh K. Shah, Grenoble, France, August 24, pp. 123-130.
36. Muzychka, Y.S. and Yovanovich, M.M., (2002), "Laminar Flow Friction and Heat Transfer in Non-Circular Ducts and Channels: Part II - Thermal Problem," *Compact Heat Exchangers*, A Festschrift on the $60^{th}$ Birthday of Ramesh K. Shah, Grenoble, France, August 24, pp. 131-139.